UCLouvain

epl

École polytechnique de Louvain

Study of the Combustion Time of Biomass Micropowder under Internal Combustion Engine Conditions

Author: **Antoine Francis**
Supervisor: **Hervé Jeanmart**
Readers: **Nicolas Parmentier, Arnaud Rouanet**
Academic year 2024–2025
Master [120] in Mechanical Engineering

ChatGPT from OpenAI was used in this work in the same way one would use a spelling or grammar assistant to help restructure sentences and correct their orthography, but never to generate or provide new information.

Abstract

Pulverized fuel is widely used in power plants and biomass micropowder can serve as an efficient biofuel by being directly injected into combustion systems. This work aims to determine the combustion time of thin pine wood particles with radii from 10 μm to 100 μm, in order to define the limiting particle size that ensures complete conversion within the time window available in internal combustion engines. This corresponds to the typical in-cylinder combustion duration of only a few milliseconds (e.g., about 7 ms at 1500 rpm, roughly 60 crank-angle degrees). The first part of this work offers an overview of biomass combustion and its current applications. The second and third parts focus on describing the phenomena occurring during the combustion and then their numerical modelling. The last part evaluates the durations of the two main phases of biomass combustion (pyrolysis and char oxidation) for varying particle sizes under various in-cylinder conditions. The results will be discussed to provide insights into practical applications.

Acknowledgments

This thesis marks the conclusion of five years of study and I would like to express my gratitude to all those who contributed to the development of this work. I would like to thank my supervisor, Professor Hervé Jeanmart, for his guidance through the completion of this thesis. I would also thank my readers, Professor Nicolas Parmentier and Arnaud Rouanet, for taking the time to review this thesis and for the valuable feedback they will provide.

I would like to thank Arnaud Rouanet for his precious advice and his constant availability.

My heartfelt thanks go to Ali for her support and the thoughtful little gifts that kept me motivated. I am also thankful to my family and friends for their unwavering encouragement during the writing of this thesis.

Finally, I would like to express my gratitude to my grandparents for their motivation and their regular encouragement during this period.

Contents

List of Figures

List of Tables

Nomenclature and abbreviations

A	Pre-exponential factor [s^{-1}] / Area [m^2]
Bi	Biot number (-)
β	Mass stoichiometric coefficient [$kg_{O_2}\ kg_C{}^{-1}$]
C_p	Specific heat capacity [J K^{-1}]
D	Molecular diffusion coefficient [$m^2\ s^{-1}$]
E	Activation energy [J mol^{-1}]
ϵ	Emissivity [-]
η	Efficiency factor [-]
h	Convective heat transfer coefficient [W $m^{-2}\ K^{-1}$]
k	Thermal conductivity coefficient [W $m^{-1}\ K^{-1}$]
K	Kinetic constant [s^{-1}]
M	Molar mass [kg mol^{-1}]
Nu	Nusselt number (-)
p_{O_2}	Partial pressure of oxygen [Pa]
ϕ	Thiele modulus [-]
R_c	Carbon ratio [kg CO/kg CO_2]
R_{char}	Char conversion rate [s^{-1}]
Re	Reynolds number (-)
R_g	Universal gas constant [J $mol^{-1}\ K^{-1}$]
ρ	Density [kg m^{-3}]
S	Surface [m^2]
Sh	Sherwood number (-)
V	Volume [m^3]

Subscripts

char	Char
conv	Convective
cyl	Cylinder
eq	Equivalent
ext	External
gas	Gas
i	Component i / Reaction i
LH	Langmuir-Hinshelwood
moi	Moisture
p	Particle
r	Radial coordinate
rad	Radiative
rel	Relative
res	Residual
spe	Specific
sph	Sphere
vol	Volatile
w	Water
w_m	Mean piston speed
z	Longitudinal coordinate
∞	Infinity

Abbreviations

AR	Aspect Ratio
CAD	Crank Angle Degree
CSIRO	Commonwealth Scientific and Industrial Research Organisation
DTG	Derivative Thermogravimetry
daf	Dry and ash free
FPP	Fast Pyrolysis Process
HR	Heating Rate
ICE	Internal Combustion Engine
LHV	Lower Heating Value
TDC	Top Dead Centre
TGA	Thermogravimetric Analysis

1 Introduction

1.1 Context and motivation

There is an increasing global demand for electricity as populations grow and technology advances. While producing large amounts of electricity is crucial, one of the major challenges the world faces today is how to store that energy efficiently. Reliable energy storage is essential to ensure a stable power supply, especially with the rise of renewable sources like solar and wind, which depend on weather conditions. Many solutions are emerging based on the same principle: using surplus electricity, produced but not immediately needed, to convert energy into storable forms. One such approach involves using excess electricity to mechanically process biomass, such as wood, by crushing or pelletizing it. This treated biomass can then be stored and later combusted in biomass power plants to regenerate electricity when demand increases. This method effectively transforms intermittent electrical energy into a stable, dispatchable energy source.

One promising method to use biomass micropowder for power generation involves adapting a diesel compression engine by replacing the conventional fossil fuel with the micropowder. In this configuration, the fine biomass particles are injected into the combustion chamber in a manner similar to liquid fuels. Exposed to the high temperatures and pressures characteristic of the compression phase, the particles auto-ignite, triggering a rapid combustion that generates the pressure needed to drive the piston.

1.2 Objectives of the study

Diesel engines used to operate at 1000-1500 rpm with high heating rates around 10^4-10^5 K s^{-1} To optimize their design, it is essential to determine the combustion duration of the particles. Since the grinding process required to obtain small particles has a significant cost as it requires more energy and specialized equipment, determining the limiting particle size is crucial. The smaller the required size, the higher the grinding energy and cost. At the same time, the combustion duration under identical in-cylinder conditions is directly linked to particle size, making it necessary to identify the largest particle radius that can still ensure complete combustion within the typical 60 crank angle degrees (CAD) time window of a diesel engine [15]. This study therefore analyses the two main combustion stages (pyrolysis and char oxidation) for a single pine wood particle with radii between 10 and 100 μm, in order to establish the maximum allowable size to undergo complete combustion under engine constraints.

1.3 General methodology

The methodology followed in this study consists of combining numerical modelling with parametric analysis to evaluate the combustion behaviour of single biomass particles. First, the in-cylinder thermodynamic conditions representative of a diesel engine are imposed, while the particle's temperature and mass evolution are computed numerically. The combustion process is divided into two successive stages: pyrolysis, modelled using *SPY*, an approach developed by J. Blondeau (2013) [4] and adapted here for very small particles under in-cylinder diesel engine conditions, and char oxidation, which is described by a kinetic–diffusive model accounting for both reaction rate and oxygen diffusion limitations. For this study, these two stages are considered separately in such a way that they do not overlap, meaning that char oxidation only starts once pyrolysis is fully completed. For each particle radius considered, the duration of both phases is determined and then summed to obtain the total combustion time. This procedure is repeated for different temperature profiles, enabling the identification of the maximum particle size compatible with full combustion within the 60 CAD window typical of diesel engines.

The specific modelling assumptions are detailed respectively in Section 5 and Section 7.

Part I

Biomass combustion: fundamentals and practical applications

2 Biomass combustion

2.1 Thermochemical conversion pathways

Biomass particles can be thermochemically converted into energy and useful products through four main processes that overlap and may occur simultaneously: drying, pyrolysis, gasification and combustion. These processes differ primarily in their operating conditions like temperature and oxygen availability and in the nature of the resulting products.

Drying is the first process where the water trapped into the particle surface begins to evaporate when the temperature inside the particle starts increasing. The water content is also called the moisture content.

Pyrolysis is the thermal decomposition of organic matter in the absence of oxygen. It typically occurs at moderate to high temperatures depending on the fuel and leads to the formation of distinct product phases. It has been shown by C. Zhang et al. [16] that sludge starts to decompose at 122.31°C, breed cane decomposed at a temperature of 203.96°C and the main pyrolysis stage occurs at 280°C for pine wood. Pyrolysis is the first step in biomass conversion and plays a central role in determining the properties of the resulting char. This process will be detailed in Part II.

Gasification takes place in a sub-stoichiometric oxygen environment, typically at higher temperatures (1000–1200 °C) [17], where the goal is to convert the solid or liquid biomass into a combustible gas mixture known as syngas, mainly composed of CO, H_2, and small amounts of CH_4. Instead of allowing complete combustion, the oxygen supply is limited to force the biomass to decompose into partially oxidized gases. Then, the produced syngas can be used for electricity and heat generation, chemical synthesis (chemical industry), or fuel production (hydrogen and biofuels). Gasification uses biomass efficiently to produce high-energy gas in a controlled process.

Combustion, by contrast, occurs in the presence of excess oxygen, with the primary objective of releasing the maximum possible heat through complete oxidation of the biomass. It mainly produces CO_2 and H_2O (with O_2 consumed), along with ash and potentially other pollutants depending on the feedstock composition. Further explanation in Part III.

Understanding the distinctions between these processes is crucial for selecting appropriate modelling approaches. In this work, we focus on drying, pyrolysis and char oxidation, which are the key stages for solid biomass conversion in engine-relevant conditions.

2.2 Characteristics of biomass

2.2.1 Structural and chemical heterogeneity

In this study, the fossil fuel is replaced by biomass, specifically pine wood. Wood is a complex material both macroscopically (wood, bark, leaves) and microscopically

(cell walls, pores). Its composition varies significantly depending on the species, the wood type (hardwood, softwood, or herbaceous), and even the part of the tree being considered. Dense hardwoods burn longer and produce more heat. Softwoods like pine ignite easier and their flame is hotter since they burn more rapidly. It is therefore relevant to briefly describe the general wood composition, emphasizing that all values used in this work are averaged from multiple experimental sources taken from Blondeau's thesis [4].

Lignocellulosic biomass [18] is structured around long linear chains of cellulose that are linked by hemicellulose chains. These chains are embedded within a lignin matrix (see Figure 1). Lignin is the longest to be decomposed during pyrolysis. Inversely, the cellulose decomposition is the fastest.

Cellulose $(C_6H_{10}O_5)_n$ is a linear glucan polymer with a high degree of polymerization (9,000–15,000 in wood), forming long fibrils (5 μm) held together by hydrogen bonds and van der Waals forces. Cellulose is the most abundant renewable organic resource on Earth as we can also find it in plants, algae, straw and reed, for example.

Hemicellulose $(C_5H_{10}O_5)_n$ is a polysaccharide matrix with a lower molecular weight and a degree of polymerization between 100 and 200. It includes various sugar units and is structurally more heterogeneous than cellulose. It accounts for about 20% of the biomass of most plants. Unlike cellulose, hemicellulose is branched.

Lignin is an amorphous, cross-linked heteropolymer that provides structural rigidity and impermeability. It is formed from three types of phenolic alcohols (coniferyl, coumaryl, sinapyl) linked by ether and C–C bonds. Lignin contributes to the natural protection of plants against threats.

Biomass samples with high lignin and cellulose contents tend to enhance pyrolysis yields by promoting the formation of tars and volatile species. In contrast, a low hemicellulose content (as observed in corn cobs) favours biochar production and slows down the degradation process during pyrolysis. More specifically, high lignin content slows the pyrolysis rate but promotes biochar formation, while high cellulose and hemicellulose contents accelerate thermal decomposition, leading to increased yields of bio-oil and non-condensable gases [11].

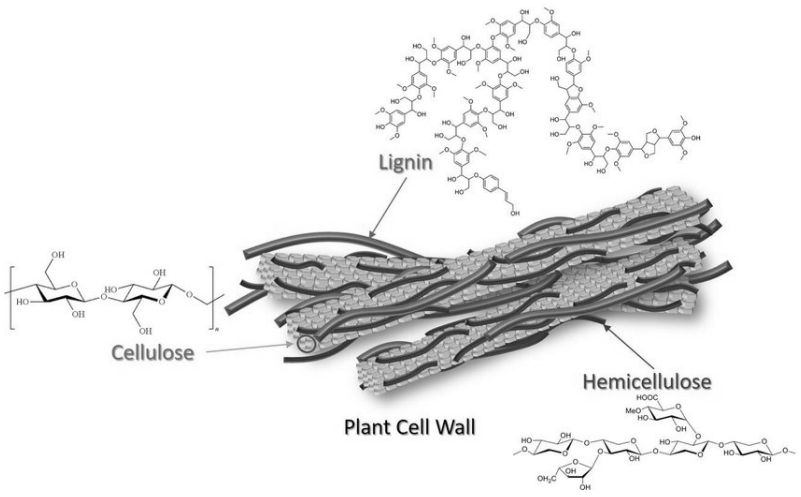

Figure 1: Structure of lignocellulosic biomass [1]

2.2.2 Moisture content and drying behaviour

All biomass resources require water to grow, and upon harvesting, they contain both free water (within cell cavities) and bound water (retained within the cellular structure). This remaining water content is called moisture and it can seriously affect the combustion rate of the material [19]: more moisture content signifies it needs more time to dry. It would require a lot of energy to completely dry an organic matter due to the water contained in its internal structure. The bigger the bound water mass fraction is, the longer the drying process duration is. As the biomass particle dries, the free water is first removed and then the bound water starts to leave the material. The total energy required to burn an organic material depends on its initial moisture content. Pyrolysis can only begin once the moisture has been fully removed; therefore, a high moisture content increases the total energy demand for both drying and pyrolysing the particle. Below is a summary of the energy required to dry an organic material [20], as might be the case in an industrial process:

- Energy is needed to heat the fuel up to 100 °C. It depends on the specific heat capacity of the fuel (2.3 kJ $kg^{-1}K^{-1}$ for pine wood)
- Energy is needed to heat the free water up to 100 °C. It depends on the specific heat capacity of water (4.184 kJ $kg^{-1}K^{-1}$)
- Energy is needed to vaporize water at 100 °C is around 2256 kJ kg^{-1}
- Energy is needed for the desorption of the bound water trapped in the biomass is around 36 to 14 kJ kg^{-1}

These high energy costs must be considered when deciding whether the organic material should be dried before use, depending on the intended application. Organic material naturally loses moisture when stored in a dry environment (warehouse) with constant air renewal (air blown by the wind), making it possible to take advantage of this "free" energy to pre-dry the material before use. This is why logs from freshly cut trees are typically left to dry for several years before being used for heating purposes, such as in domestic wood stoves. On an industrial scale, biomass particles are dried in large storage facilities where a continuous flow of air removes moisture. This airflow is constantly renewed to maintain an efficient drying environment and prevent saturation with humidity. A moisture content of around 14% is generally obtained within 60 to 90 days when air-dried [21].

2.2.3 Proximate analysis, ultimate analysis and ash-forming species

Proximate and ultimate analysis are used to characterize the properties of the biomass. Proximate analysis determine the composition in volatile matter, moisture content, fixed carbon content and ash. Ultimate analysis gives the elementary components of the biomass (i.e. C, H, N and O). According to E. Alakangas [22], volatile matter concerns the gaseous species mainly emitted during the decomposition of cellulose and hemicellulose (tars and light gases) and is the major constituent in biomass (usually between 60 to 85%). The fixed carbon content is the residual solid matrix remaining after the pyrolysis and it ranges from 10 to 25% (or more) depending on the environment conditions. After the completion of the combustion of the volatiles and the fixed carbon content, there is a residual matrix that cannot be burnt: it is called ash. For biomass like wood, the ash percentage is very low

(around 2 to 5%) and can be around 0.1% for pine. It is even bigger for herbaceous biomass like wheat straw and rice husk ($> 10\%$). Various analysis for biomass samples are depicted in Appendix A.

2.2.4 Reference biomass

For the remainder of this study, pine wood is chosen as the reference biomass. Pine is widely used in combustion applications, notably because its auto-ignition temperature, around 427°C [23], is relatively low compared to the typical in-cylinder temperatures of a diesel engine, which facilitates ignition. In addition, pine wood is characterised by a low ash content, which represents a significant advantage since ash formation can lead to long-term operational issues in internal combustion engines [24]. Moreover, pine is also abundant and well-documented in the literature making it an appropriate reference in this work. The pine wood composition used for the combustion models is from averaged experimental data and is taken from Blondeau's work [4].

2.3 Influence of operating conditions

The behaviour of biomass particles during thermal decomposition is highly sensitive to external conditions. Key parameters such as surrounding temperature and the particle temperature, pressure, heating rate, particle size and shape influence the reaction kinetics, the heat and mass transfer and the efficiency of the conversion.

2.3.1 Temperature, heating rate and pressure influences

Temperature is a dominant factor in determining the rate of pyrolysis and char oxidation. Higher temperatures accelerate both volatile release and carbon oxidation but it may lead to thermal runaway if the heat release is higher than the dissipation rate. Incomplete conversion can still occur if the residence time is insufficient. The heating rate plays a crucial role, especially in fast and flash pyrolysis [25], where high rates ($>$1000 Ks^{-1}) favour liquid and gas formation over char. The particle does not heat up or cool down as quickly as the surrounding gas. Depending on the magnitude of the heating rate, the particle may or may not reach a sufficiently high temperature to initiate char oxidation. Pressure also influences reaction kinetics and gas diffusion ($D \propto 1/P$) [26]. Elevated pressures, as found in internal combustion engines (> 60 bar), can suppress volatile release [27], enhance secondary reactions, and reduce the diffusivity of oxygen, thus altering the overall combustion behaviour. As will be discussed later in this work, the overall reaction rate can be limited either by intrinsic chemical kinetics or by the rate of oxygen diffusion to the particle surface. Under elevated pressure, the reduced diffusivity becomes the dominant limiting factor, meaning that even very small particles may become diffusion-controlled.

2.3.2 Influence of particle size and shape

Under identical conditions, two particles of different size will not thermally decompose at the same rate. A larger particle contains more material to degrade and requires more time for heat to reach the core. The Biot number allows to characterize a particle as thermally thin or thermally thick as a function of its size:

$$Bi = \frac{h_{eq} L}{k_{eq}} \tag{2.1}$$

with L the characteristic length ($L = \frac{V}{A}$ $[m^3m^{-2}]$), h_{eq} and k_{eq} the convective heat transfer coefficient and the thermal conductivity of a particle respectively. If its *Biot* number is smaller than 0.1, the particle is considered thermally thin.

In the case of this study, the particle radii range from 10 to 100 μm. It is generally assumed that particles with diameter ≥ 100 μm (i.e radius ≥ 50 μm) are considered thermally thick. A thermally thin particle means that there is no thermal gradient within the particle: it heats up uniformly. The particle size is especially critical in engine-relevant conditions, where complete thermal conversion must occur within a few tens of milliseconds.

2.3.3 Effect of oxygen concentration and gas flow

While pyrolysis primarily occurs under low oxygen concentrations, the availability of oxygen is a key factor in governing the rate and completeness of char oxidation. Insufficient oxygen can significantly slow down the reaction and extend the burnout time. Conversely, high oxygen concentrations tend to accelerate oxidation but may lead to premature ignition, compromising combustion control. In the case of internal combustion engines, precise control of the combustion rate is essential to improve efficiency, reduce emissions, and prevent engine damage caused by knocking or excessive heat [28]. In addition, the gas flow surrounding the particle influences both convective heat transfer and oxygen transport. Turbulent flow, in particular, enhances mixing and improves heat and mass transfer. These factors are critical when designing biomass injection and combustion strategies within confined geometries, such as internal combustion engine chambers.

2.3.4 Time constraints for combustion in ICEs

The combustion time of biomass microparticles in internal combustion engine conditions is constrained by the short duration available at high temperature within the engine cycle. At 1500 rpm, efficient operation requires that combustion must be completed within approximately 7 ms, equivalent to about 60 crank angle degrees [15]. Micronized biomass particles heat rapidly during compression, with heating rates of 10^4–10^5 K/s, reaching gas-phase temperature and initiating heterogeneous surface oxidation within a few milliseconds. CO formed in this early stage can then undergo homogeneous combustion near top dead centre. For particles above a certain critical diameter (quantified later in this work), heating is slower and residence time at sufficient temperature is inadequate, freezing heterogeneous reactions during expansion and limiting conversion. Literature [14] reports from drop tube furnace experiments on particles smaller than 250 μm (ranging 70 to 250 μm) indicate volatile burning durations ranging from 10 to 80 ms and fixed carbon burning times between 8 and 60 ms. Such durations are often incompatible with the short residence times available in ICE operation, unless particle sizes are further reduced or in-cylinder conditions are intensified: this approach will be investigated in the present work.

3 Applications: engines operating on biomass micropowder

In 2013 [2], the transport sector consumed 62% of global oil and remained 96% dependent on it, highlighting the urgent need for alternative fuels. Classical biofuels like biodiesel and bioethanol offer limited substitution potential (less than 10%), whereas thermochemical routes (e.g., Gas-to-liquid/Biomass-to-liquid) may reach up to 27% by 2050. Among renewable options, biomass (wood, algae, agricultural and industrial residues) stands out due to its CO_2 neutral profile (often debated), wide availability, high volatile content and low ash content. While current biomass-to-energy technologies mostly rely on producing gaseous or liquid fuels through complex and costly processes, the direct use of dry biomass powder in reciprocating engines has seen little exploration. Although coal dust was historically tested in ICE starting with Rudolf Diesel's early experiments, no technology has achieved industrial success due to challenges with fuel handling, wear, and injection.

Biomass powder offers significant advantages over coal [29], including lower ash and sulphur contents, higher volatile matter which favours ignition and a more reactive char with greater specific surface area. These properties make finely ground biomass a promising solid fuel for internal combustion engines, particularly in strategic contexts such as decentralized energy systems, power generation when renewable sources cannot meet demand or simply to produce electricity in areas with limited infrastructure. Solid biomass is generally less flammable than liquid fuels and easier to store. However, in both cases, storage and handling are subject to specific safety measures to prevent accidents (see Subsection 3.2).

3.1 History of solid fuelled internal combustion engine

The following provides a concise overview of the main advancements in the development of solid-fuelled internal combustion engines. The development of these engines has spanned over a century and can be divided into three major phases [2]:

1. 1892-1945: dry coal dust in Germany and Japan
   Efforts began with Rudolf Diesel who tested coal dust as fuel. Significant progress was made by R. Pawlikowski and some German manufacturers who developed engines operating on dry pulverized coal using prechambers, compressed air injection (> 60 bar) and wear resistant materials. Japan also worked on automotive applications but faced technical issues like injector clogging and wear.

2. 1945-1973: coal-diesel and coal-water slurries
   After the Second World War, the U.S. shift toward diesel fuel mixed with water or water and slurries to ease injection. While wear and combustion stabilities were still concerning, the conventional injection systems could be used. Unfortunately, efficiency and emissions were worse than with diesel.

3. 1973-Today: Slurry-based fuels
   After a period of reduced interest in solid-fuelled internal combustion engines due to stable crude oil prices in the 1990s, recent years have seen renewed attention toward slurry-based fuels. In 2004, a Swedish-Finnish-Danish project

tested wood dust fired diesel engines but it was stopped after 28 hours due to extreme thermal stress that cause the engine melting [30]. An Australian CSIRO study in 2008 identified diesel applications as promising, leading to the development of a low-speed (200–600 rpm) Direct Injection Coal Engine (DICE) fired with coal–water slurry [31]. In 2010, Patton et al. [32] proposed to use wood charcoal instead of mineral coal, which reduces wear thanks to lower ash content and can be further processed by water leaching to match diesel's ash levels (100–1000 ppm). In 2011, Soloiu et al. [24] conducted an experimental study using a 25% cedar-char–diesel slurry in a Yanmar NF-19 engine. They reported performance similar to pure diesel, with comparable ignition delays, higher net heat release and approximately 30% higher NO_x emissions, while wear remained negligible. Collectively, these findings indicate that slurry fuels, particularly those derived from biomass char, can achieve performance levels close to diesel while addressing wear concerns, although challenges related to emissions and high-temperature durability persist.

3.2 Current limitations

Using biomass is an effective way to reduce fossil fuel consumption. However, there are still technical limitations that must be addressed before it can be used directly in compression engines primarily designed for liquid fuels such as diesel:

1. *Fuel feeding*
   One of the major concern is to ensure a constant flux of solid particle. Microparticles can clump together inhibiting the advantage to have very small particle size. Micropowder can lead to sludge formation to the contact with lubricated surfaces and to frequent injector clogging. Some solutions have already been explored like customised injector and a better control over the particle size used.

2. *Wear*
   Wear is an important challenge to face to ensure the longest possible working life of the engines. Unlike coal whose ash contains abrasive oxides that can lead to excessive wear of the engine components, biomass generally contains less ash and fewer abrasives suggesting a lower wear risk.

3. *Ignition control*
   Due to the different phases solid fuels undergo (such as drying, pyrolysis, volatile combustion, char burnout), the total combustion time is longer than conventional fuel. Some solutions have been developed to reduce the ignition delay: increase the intake temperature, use of thermally insulated prechambers, high pressure powder injection to enhance air turbulence and thus mixing and ignition.

4. *Compression ratio*
   A compression ratio optimised for diesel combustion (generally between 14:1 and 25:1) is much higher than the optimal compression ratio for biomass-fuelled engines (around 3.5:1). While such a compression ratio is too low for diesel auto-ignition, it is still sometimes insufficient for certain biomasses with slow heat release, meaning they may require even higher compression or preheating to burn effectively [33]. To counter this, the study of G. Suanes et al. suggests turbocharging to increase air intake temperature. This adaptation

could raise efficiency up to 35% and thus bringing biomass engines closer to diesel performances despite their inherent limitations.

Storage [34] is a practical and safety constraint in the deployment of biomass as a solid fuel. Biomass is consumed during the whole year but its harvesting is only seasonal. Storage is the best solution to counter this supply-demand gap. Biomass powder is particularly sensitive to moisture and microbial degradation and spontaneous heating. Microparticles, due to their surface area and low density, are prone to absorbing ambient humidity which accelerates microbial activity and material decomposition. Moreover, their flammability increases when dry, while wet conditions can favour self-heating and sometimes lead to fire or dust explosion hazards in confined storage without ventilation systems.

From a logistical perspective, powdered biomass requires more sophisticated infrastructures than pellets and logs. Traditional open-air warehouses offer a poor protection against environmental factors. Enclosed and climate-controlled steel silos are more appropriate but are much more expensive to build and to operate. Storage must also consider aeration to limit self-heating, mould growth and dust agglomeration, which is the primary cause of explosions. Compromises must be made between storage cost, safety and fuel quality. Especially for biomass intended to be used in internal combustion engine under controlled conditions.

3.3 Reference engines

To ensure consistency with a reference engine and allow comparison with the experimental results of L. Stover et al. [14], the modelling parameters were matched to the specifications of the Hatz 1D81 diesel engine. Since the temperatures reported in Stover's study are relatively low, thus restricting the experimental window, additional data were taken from a recent study (2019) on the influence of engine speed variations in a single-cylinder diesel engine [9]. This latter source provides relevant pressure and temperature values that are used in the present work. The main difference between the two studies lies in the fuel used: the Hatz engine experimental data were obtained using biomass whereas the engine speed variation study was conducted with diesel. This explains the temperature difference between the two. For informational purposes, the data sheets of both engines are reported in Appendix B.

Part II
Biomass pyrolysis

4 Theoretical background

When a solid or a liquid fuel is exposed to a significant increase in temperature, it undergoes thermal decomposition: a process where chemical bonds are broken by heat. This decomposition proceeds through several stages and the first major step is typically pyrolysis.

In the absence of oxygen in the surrounding gas phase (i.e. under inert or low-oxygen conditions) and when the particle reaches a temperature around 150°C [16], it thermally decomposes into a mixture of volatile gaseous species and a solid carbon-rich residue. The volatile species consist mainly of high molecular weight compounds called *tars* and *light gases*. The solid residue left behind, particularly in the case of solid fuels like biomass, is referred to as *char* [20]. In literature it is postulated that devolatilization is a first-order reaction process [35].

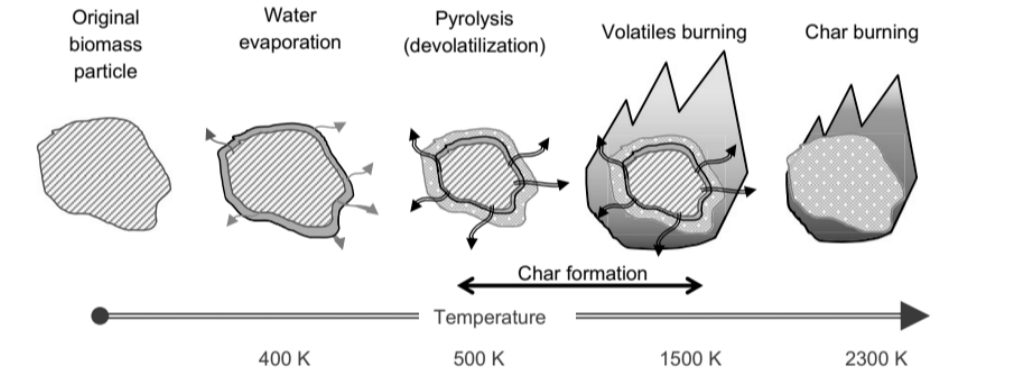

Figure 2: Processes of solid fuel combustion [2]

4.1 Fast and Flash pyrolysis

Fast and flash pyrolysis are considered when the process happens under high heating rates. The increasing interest in fast pyrolysis processes stems from their potential to efficiently convert biomass into liquid products. Fast pyrolysis typically operates under high temperatures (450–800 °C) and short residence times (0.5–10 s) [36]. These conditions minimize the involvement of volatile compounds in secondary reactions, thereby limiting the cracking of primary products and promoting higher bio-oil yields. Effective deployment of fast pyrolysis would require high rate of heat transfer, which can be attained by retaining a fine particle size. As the reaction is expected to take place in a very short time, the chemical kinetics along with rate of mass and heat transfer and transition phenomena play a key role in fast pyrolysis. Flash pyrolysis can be considered similar to fast pyrolysis, but in an intensified form. In fact, the heating rates are higher than 1000 °C s^{-1} and the working temperature around 800–1200 °C. Moreover, the operational parameters that are often employed are the size of the particle (< 0.1 mm) and a short residence time. Flash and fast pyrolysis are often regarded as similar thermochemical conversion technologies. However, flash pyrolysis is distinguished by its ability to minimize or eliminate biochar formation, focusing almost entirely on maximizing liquid yields.

4.2 Thermal processes and governing parameters

In the following section, the drying phase and the release of volatiles are discussed. The behaviour of the fixed carbon thermal degradation, and the role of ash content will be addressed later in the section dedicated to char oxidation (see Section 6).

4.2.1 Drying

In order to improve the combustion efficiency and maximize the yield of high-energy fraction such as bio-oils, biomass is often industrially pre-dried. Moisture content is typically reduced to 3-10% before thermal conversion. When the particle reaches 100°C, water starts being released off the particle by evaporation. Water in biomass takes two forms: free water and bound water. Free water refers to water that is not chemically bound to other molecules and that is in liquid or in vapour form within the cell cavities while bound water is part of the cell wall materials. During this endothermic process, the particle loses first the free water from the cell cavities, which do not shrink the cell and the particle keeps its shape. The deformation starts once the bound water starts to leave the cell wall as the particle dries further.

"*Bound water or moisture is the minimum water held by the material that exerts an equilibrium vapour pressure less than the pure water at the same temperature.*"[37]

The simplest approach to modelling moisture evaporation is to use a first-order kinetic evaporation rate, typically represented by the following chemical expression:

$$\text{Moisture} \rightarrow \text{Water vapour} \tag{4.1}$$

According to the J. Blondeau's thesis [4], Bellais compared three different drying models and concluded that the single-reaction model, while highly simplified, does not lead to significant accuracy loss when applied under high heating rate conditions. Its ease of implementation makes it particularly attractive for complex simulations where drying is not the primary focus. Although high heating rates may cause some deviation in the drying behaviour, such as a broader temperature range for moisture release, the associated time delay remains minimal. It does not significantly affect the subsequent pyrolysis process. Most importantly, the key thermal effect of drying (the heat of vaporization consumption) is adequately accounted for in this simplified model. The drying phase follows the Arrhenius law:

$$\frac{dm_{H_2O}}{dt} = -A_{moi} \cdot exp\left(-\frac{E_{moi}}{R_g T}\right) \cdot m_{H_2O}\ [kg\ s^{-1}] \tag{4.2}$$

The influence of moisture content on the duration time is illustrated in Figure 3 taken from the work of J. Blondeau [4]. Due to the increase of moisture content, the temperature takes more time to reach the centre of the particle and as expected the conversion time increase.

Finally, although no chemical transformations are assumed to occur during the drying phase, this stage plays a critical role in the overall conversion process. By removing the inherent moisture content, it facilitates heat transfer to the solid matrix and thus enhances the onset of pyrolysis (devolatilization). The moisture content thus directly influences the energy balance and the timing of upcoming chemical reactions.

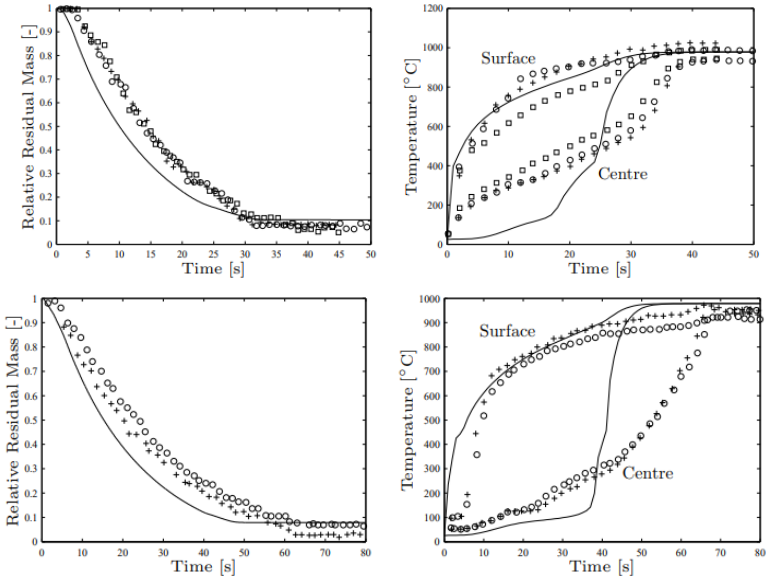

Figure 3: (Top) Pyrolysis of a poplar cylindrical particle with a moisture content of 6%, with $AR = 1$, $d = 9.5$ mm. (Bottom) Pyrolysis of a poplar cylindrical particle with a moisture content of 40%, with $AR = 1$, $d = 9.5$ mm. Relative residual mass and temperature profiles vs. time: predictions from SPY (solid) and experimental results from Lu [3] (markers). Figure taken from J. Blondeau's thesis [4]

4.2.2 Thermal decomposition and volatile release

The completion of biomass pyrolysis occurs through a series of thermally activated decomposition steps, which can be clearly identified when analysing the relative mass loss rate in s^{-1} unit. The thermal degradation of the volatiles is defined in SPY in the same way as for the drying step:

$$\frac{dm_{vol_i}}{dt} = -A_{vol_i} \cdot exp\left(-\frac{E_{vol_i}}{R_g T}\right) \cdot m_{vol_i} \; [kg \; s^{-1}] \tag{4.3}$$

The overall mass conversion results from the cumulative contributions of the individual mass losses associated with each volatile species, each of which follows its own decomposition pathway and rate of release.

The first peak corresponds to the evaporation of bound water, commonly referred to as the drying phase. This is followed by two major overlapping peaks associated with the degradation of hemicellulose and cellulose, the two most reactive components of lignocellulosic biomass.

Hemicellulose, being the most thermally sensitive, begins to decompose at relatively low temperatures (200–300°C), while cellulose, which is typically the most abundant component, undergoes rapid decomposition between 300 and 400°C. This stage is also characterized by the significant emission of volatiles, including condensable tars and permanent gases. Occasionally, a shoulder can be observed on the descending side of the cellulose mass flux peak, which is attributed to the degradation of secondary hemicellulose species.

A final peak in the mass loss rate curve is associated with the release of trapped

species, such as light gases, additional tar, and volatiles originating from lignin. Unlike hemicellulose and cellulose, lignin decomposes more slowly, over a broader temperature range typically spanning from 250 to 600°C. This broad degradation profile overlaps with other components and is especially pronounced in particles larger than 1 mm diameter, where internal heat and mass transfer limitations delay the release of trapped volatiles.

These various volatiles release stages occurring during the pyrolysis process are clearly observable in Figure 4.

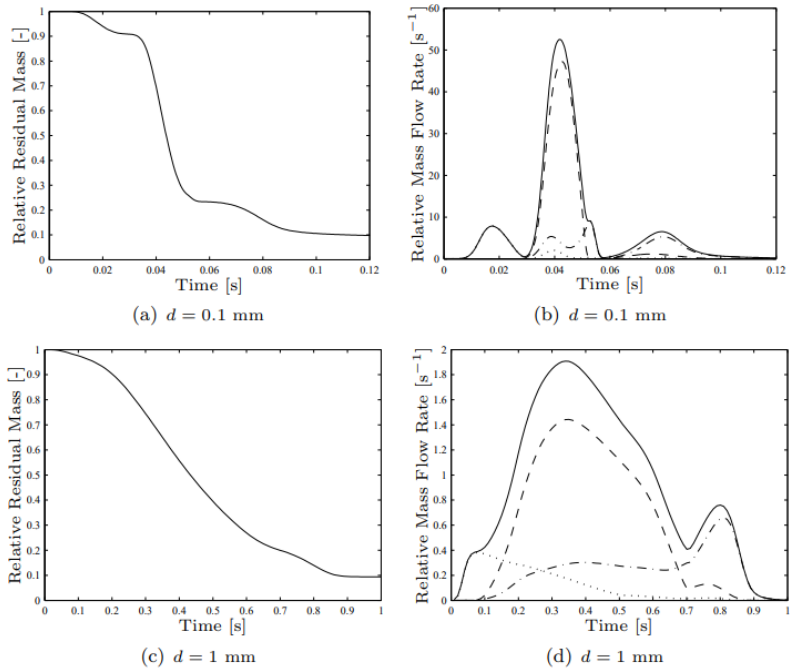

Figure 4: Relative residual mass and relative mass flow rate vs. time: (a,b) thin particle, and (c,d) thick particle. The total mass flow rate (solid) is composed of tar (dash), gas (dash-dot) and steam (dot). Figure taken from J. Blondeau's thesis [4]

Following this devolatilization process, a solid carbonaceous residue remains. It is commonly referred to as char. This residue, mainly constituted of fixed carbon and inorganic ash, marks the transition from pyrolysis to the subsequent oxidation stage. In thermal models, the end of the third peak in the relative mass flow rate curve can be used to estimate the characteristic timescale of pyrolysis. Experimental and literature data [38] suggest that the fixed carbon content of wood-based biomass typically ranges from 5% to 35% of the initial mass. This remaining fraction is considered representative of the fixed carbon, although it may still contain traces of residual tar or heavy volatiles.

4.2.3 Influence of pressure and temperature

According to the study by Q. Wang et al. [39] about the effects of pressure on kinetic parameters during pyrolysis and gasification of corn stovers, increased pressure has been shown to enhance the probability of intermolecular collisions, thereby promoting reaction rates. On the other hand, pressure also inhibits the release of volatile species, reflected by the increase in apparent activation energy under high-pressure conditions. Nonetheless, thermogravimetric analysis indicates that the promoting

effect of pressure outweighs its inhibiting influence. As a result, both pyrolysis and gasification tend to react more completely under elevated pressure.

It is known that the devolatilization reaction rate is simulated using an Arrhenius-type equation as the thermal decomposition of biomass is governed by temperature-dependent chemical kinetics. High temperatures significantly increase the exponential term $exp\left(\frac{-E_a}{R_g T}\right)$, thereby accelerating the reaction kinetics. The higher the temperature, the more the biomass is converted into volatiles compounds and gases, leaving less solid residue [40].

4.3 Expected pyrolysis products from biomass decomposition

As explained above, the composition of biomass can vary significantly depending on the species, growth conditions, and treatment processes. Once the biomass undergoes drying, pyrolysis and combustion, its decomposition can be characterized through the following parameters:

- Moisture content impacts the duration and energy demand of the drying phase.
- Volatile contents are the gaseous species emitted during pyrolysis under the form of tars and light gases. It has been reported that large volatile content promote ignition which is relevant for ICE applications.
- The fixed carbon content is the residual solid matrix after completion of pyrolysis. It is mainly composed of carbon and it is commonly referred to as char. As the temperature continue to increase or remains high enough, it can further be decomposed and emits volatiles. Also, considering an arbitrary duration for the pyrolysis, the fixed carbon content is the residual mass after the devolatilization stage.
- Ash content is a residual solid after complete combustion of all the volatiles and fixed carbon. Even if biomass fuels generally have lower ash content, ash remaining in the engine chamber can be easily removed by water leaching [2].

Pyrolysis process of biomass produces three main fractions: bio-oil (liquid), volatile species such as tars (heavy hydrocarbons) and light gases (carbon monoxide (CO), carbon dioxide (CO_2), hydrogen (H_2) and methane (CH_4)) and char, a solid carbon residue. The distribution of these products strongly depends on the operating conditions, particularly the heating rate, temperature, and residence time. Maximizing bio-oil yield (as in fast pyrolysis) requires high heating rates, short residence times, and fine biomass particles. These conditions limit secondary cracking reactions that would otherwise convert volatiles into gas or char. Optimal temperatures for bio-oil production typically range around 500 °C. On the other hand, slow pyrolysis conditions (lower heating rates, longer residence times) favour biochar formation, making it suitable for applications such as soil amendment, carbon sequestration or solid fuel.

There is therefore a trade-off between bio-oil and biochar yields, as increasing one typically reduces the other. For internal combustion engine applications, the fact that combustion must occur very rapidly (in general within 60 CAD), and in addition, the high in-cylinder temperature range tend to enhance bio-oil yields.

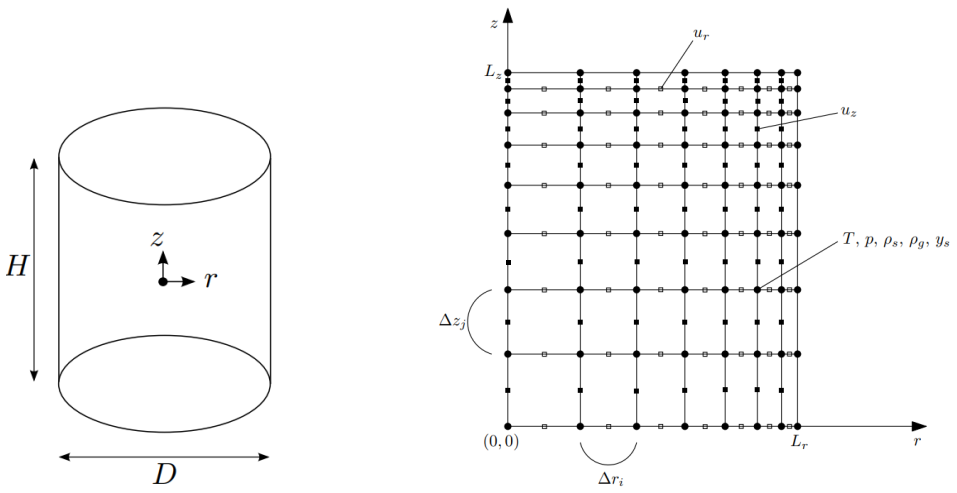

(a) (b)

Figure 5: (a) Schematic of the simulated cylindrical particle in *SPY*. (b) General form of the computational mesh. Both figures are taken from [4]

5 Numerical modelling of pyrolysis

The single particle pyrolysis model *SPY* used in this work has been developed by J. Blondeau [4] and parameters will be modified in order to be conformed to the numerical experiment objective.

SPY use an improved Ranzi et al. mechanism [41] to simulate the devolatilization behaviour of the particle. This mechanism is a comprehensive and detailed model consisting of a set of primary reactions describing the devolatilization of solid biomass, coupled with homogeneous gas-phase reactions for volatile cracking and oxidation. This detailed approach enables accurate prediction of both mass loss and chemical composition of the volatiles species. Coupled with the thermal and mass transfer modules within *SPY*, it allows for spatially and temporally resolution of the particle's internal behaviour under various thermal conditions. This makes the model particularly well-suited for accurate analysis of pyrolysis processes in engine conditions, by instance.

5.1 Particle modelling

5.1.1 Particle geometry

The conservation equations have been considered in cylindrical coordinates and axisymmetry is considered. The pyrolysis model is thus two-dimensional, enabling the representation of both the geometry and the anisotropic nature of fibrous biomass materials. It is well established that thermal conductivity and permeability differ significantly along the fibre direction compared to the transverse direction [4]. Moreover, it is assumed that the particle is perfectly milled and has passed through a sieve, ensuring a uniform size distribution. The particle is then modelled as a cylinder (see Figure 5a) with its diameter equal to its height. This geometric simplification is introduced to focus specifically on small particles. The aspect ratio defined as $AR = \frac{H}{D} = \frac{L_z}{L_r}$ with L_z the half-height of the particle and L_r the radius is then equal to 1.

5.1.2 Particle size and mesh

In this study, the *SPY* model is used to evaluate particle radii ranging from 10 to 100 μm. These specific values were selected to encompass both previously studied larger sizes [14] and smaller sizes of interest, with the aim of identifying a limiting particle dimension suitable for compliance as a potential new fuel in typical diesel engines. The computational mesh is adapted to the size of each particle to balance accuracy and computational cost. Larger particles allow the use of coarser meshes, whereas applying the same discretisation to smaller particles would be too computational costly. To maintain numerical stability and accuracy, the mesh resolution is adjusted with particle size, and for particles with radii below 40 μm, a reduced mesh is employed. This implies a deliberate loss of spatial detail such as for the temperature distribution inside the particle, which is acceptable in the present context since only the total thermal decomposition time is of interest, rather than the detailed volatile release profile. The general form of the computational mesh is illustrated in Figure 5b.

5.2 Single particle environment conditions

Very small particles can be considered thermally thin. It means that heat can diffuse through it much faster than the timescale of the heating process: heat diffusion is quasi instantaneous and the heating is uniform through the particle, temperature gradients are negligible. This is not the case for the larger particle which are thus characterized as thermally thick. In general, particles whose radius is ranging between 10 μm and 50 μm are considered thermally thin and their Biot number is assumed lower than 0.1. This behaviour is evident in the results section, where larger particles exhibit slower mass loss, indicating that heat penetration into the particle is more limited.

The initial goal of the model was to simulate the combustion behaviour for pulverized fuel boiler. The fuel particles were subject to important heating rates at atmospheric pressure. In this study, the in-cylinder pressure of an ICE increases in such a way that the temperature highly increases for a very short period of time. In general, it is assumed that combustion should ideally occur within less than 60 CAD [15]. Therefore, the time available for combustion decrease with engine speed: 10 ms at 1000 rpm and about 6.66 ms at 1500 rpm. In order to improve the engine performance the combustion duration is required to be short so that all the charge undergoes complete burning.

5.2.1 Boundary conditions for heat and mass transfer

In the *SPY* model [4], the pressure at the domain boundaries is assumed to match the ambient external pressure. Regarding the species transport, the composition in the external boundary layer is taken equal to that at the particle surface, corresponding to a purely convective mass transfer toward the surrounding gas. This assumption leads to the application of Neumann boundary conditions imposed on

all mass fraction y_i at the outer radial and axial boundaries:

$$\left.\frac{\partial y_i}{\partial r}\right|_{(r=L_r,\, z)} = 0 \tag{5.1}$$

$$\left.\frac{\partial y_i}{\partial z}\right|_{(r,\, z=L_z)} = 0 \tag{5.2}$$

In addition to the symmetry condition naturally imposed at $r = 0$ by the cylindrical coordinate system, symmetry is also assumed in the longitudinal direction at the centre of the particle ($z = 0$):

$$\left.\frac{\partial \phi}{\partial z}\right|_{(r,\, z=0)} = 0 \tag{5.3}$$

for any scalar field ϕ such as temperature, species concentration or pressure.

For simplification purposes, the typical in-cylinder pressure variation is not included in the present version of *SPY*, which was originally designed to operate under atmospheric conditions.

Since temperature plays a dominant role in controlling the pyrolysis reaction rate through the Arrhenius law, the in-cylinder temperature evolution has been integrated into the model. This catalytic effect compensates the absence of pressure variation and ensures that the simulation remains reasonably representative of realistic conditions encountered in internal combustion engines.

5.2.2 Heat transfers

The objective is to simulate the chamber conditions in a typical diesel engine. The temperature and time values used in this study were taken from the internal measurements reported in [14] about the Hatz 1D81 diesel engine and from the work of U. Rajak and T. Verma [9]. The gas starts being compressed and its temperature rises. The assumed adiabatic compression process results in an important increase in temperature in the cylinder and it can be computed using the ideal gas relation:

$$P = \frac{nR_gT}{V} \tag{5.4}$$

$$PV^{\gamma} = K = constant \tag{5.5}$$

With $\gamma = \frac{C_p}{C_v}$ the ratio of the specific heats of the gas (air in this case) respectively at constant pressure and constant volume. This ratio is generally equal to 1.4 for air. The final temperature is determined using the ideal gas law. For typical diesel engine compression ratios (14:1 to 25:1), compression alone can raise the temperature to approximately 1000 K. After the fuel injection, the temperature rises sharply as ignition occurs. During the exhaust phase, both the internal temperature and pressure drop, thereby restoring the initial conditions for the subsequent cycle.

When the particle is injected in the combustion chamber (approximately 21.5 CAD before TDC), the latter is heated up by its environment. The single particle is subjected to two main heat transfers:

- Radiative heat transfer q_{rad} refers to the heat flux exchanged between the

cylinder walls (e.g., in an internal combustion engine) and the particle surface. The corresponding radiative heat transfer coefficient is defined as:

$$h_{\text{rad}} = \frac{q_{\text{rad}}}{T_{\text{rad}} - T_w}$$

where T_{rad} is the temperature of the radiative heat source.

- Convective heat transfer q_{conv} represents the heat flux transferred from the surrounding gas to the particle surface. The convective heat transfer coefficient is given by:

$$h_{\text{conv}} = \frac{q_{\text{conv}}}{T_\infty - T_w}$$

where T_∞ denotes the bulk gas temperature far from the particle.

An equivalent heat transfer coefficient is considered:

$$h_{\text{eq}} = h_{\text{conv}} + h_{\text{rad}} = \frac{q_{\text{conv}}}{T_\infty - T_w} + \frac{q_{\text{rad}}}{T_{\text{rad}} - T_w}$$

As explained above, the particle surface temperature does not heat up at the same rate as the gas. The particle is subject to an equivalent heat flux $q_{\text{eq}} = q_{\text{conv}} + q_{\text{rad}}$. The radiative contribution to the heating is less significant than the convective one and is considered to be the primary contributor to the residual heat present in the cylinder. The heat flux is then taken to be purely convective: $q_{eq} = q_{conv}$.

An appropriate approach to compute the value of h_{conv} consists in using classical correlations based on the Nusselt number, such as the Ranz–Marshall correlation. This correlation provides realistic estimates of the convective heat transfer coefficient by accounting for local flow conditions around the particle, including Reynolds and Prandtl effects. As a result, they offer a physically accurate description of the heat exchange between the hot gas and the biomass particle surface. The Nusselt number correlation for a flow around a sphere is the following:

$$Nu = 2 + 0.6 \cdot Re^{\frac{1}{2}} \cdot Pr^{\frac{1}{3}}$$

Assuming that the relative velocity between the solid and the gas phase is low and considering the small size of the particle, the Reynolds number can be neglected. Under these conditions, the flow corresponds well to a Stokes flow regime and the equation simplifies into Nu $\approx$ 2. The local equivalent heat transfer coefficient can be computed as:

$$h_{eq} = h_{conv} = \frac{2\lambda}{L} \tag{5.6}$$

where L is the characteristic length of the particle [m] and λ is the thermal conductivity of the gas (air) $[Wm^{-1}K^{-1}]$. The air thermal conductivity is assumed to be approximately 0.063 $Wm^{-1}K^{-1}$. This value was taken from *The EngineeringToolBox* website [42], based on computed data at various temperatures under atmospheric pressure. Since thermal conductivity is weakly dependent on pressure, it is assumed to remain constant throughout the engine cycle. In this specific case, the particle size is the only parameter influencing the convective heat transfer coefficient.

The temperature evolves along the radial and axial directions (for z=0 and r=0, respectively). Following the model, the isothermicity behaviour of the thin particle is well represented by the model as there is only a difference of a few tens of degree between the surface and the core temperature. It should be noted that the temperature at the particle's corner (i.e., at r=L_r and z=L_z) is systematically higher than the values presented, resulting in a temperature gradient along the particle's diagonal (from centre to corner) that is twice as steep as along the central axes [4].

5.2.3 ICE conditions implementation

To better reflect the conditions inside an internal combustion engine, an in-cylinder gas temperature profile is imposed. Due to the limited availability of experimental data [14, 9, 43], using average heating rates provides a good approximation of the thermal environment conditions.

As explained and assumed above, the single particle is heat up thanks to an external heat flux q = $h_{conv} \cdot (T_{gas} - T_p)$ where T_p is the temperature at the particle surface. Two scenarios are modelled: the first approximates the in-cylinder conditions of a biomass-fuelled compression engine [14], while the second represents the more realistic operating conditions of a diesel-fuelled engine [9, 43].

1. *Engine-like dynamic heating (biomass-fuelled)* (Figure 6) represents a more realistic scenario in which the gas temperature follows a typical internal combustion engine profile. After reaching its peak value, the gas temperature rapidly decreases to 373 K. The resulting heat flux drives the particle surface temperature to rise as much as possible during the heating phase and then to release heat at a comparable rate during the cooling phase.

2. *Engine-like dynamic heating (diesel-fuelled)* represents the scenario of a single particle subjects to the in-cylinder conditions of an engine running with diesel. Such engines exhibit higher temperatures during the compression and ignition phase, with peak in-cylinder temperature reaching approximately 3000 K. As in-cylinder temperature increase with engine speed [9], three subcases are simulated in order to study the influence of various temperature profiles in the combustion duration.

To illustrate the temperature profiles and the convective heat flux applied to the single particle in each scenario, their respective graphs can be found at the end of this section. The simulation starts at the moment of particle injection.

According to Blondeau [4], the heat capacity of biomass, c_p [J kg $^{-1}$K^{-1}], varies with temperature and is given by:

$$c_p = 2300 - 1150 \cdot \exp\left(-0.0055 \cdot (T - 273)\right) \tag{5.7}$$

This heat capacity is the only one used in the particle temperature profile computation, as it has a more significant influence than those of the gaseous species.

5.3 Mass transfer modelling

The particle geometry and shape are now modelled with its surrounding environmental conditions. The particle mass decrease as moisture is removed and volatile

Component	Heat capacity c_p $[\,\mathrm{J\,kg^{-1}\,K^{-1}}\,]$
Char	$1430 + 0.355\,T - 7.32 \times 10^7\,T^{-2}$
Tar	$1800 - 800\,\exp\left(-0.0055\,T\right)$
Gas	$770 + 0.629\,T + 0.000191\,T^2$
Air	$950 + 0.188\,T$

Table 4: Heat capacities of different components. Table from J. Blondeau thesis [4].

components are released. The overall mass loss rate is computed from an Arrhenius-type expression:

$$\frac{dm_i}{dt} = -A_i \cdot \exp\left(-\frac{E_i}{R_g T}\right) \cdot m_i \tag{5.8}$$

where m_i is the mass of species i, A_i the pre-exponential factor, E_i the activation energy, R_g the universal gas constant and T the particle temperature. This formulation couples heat and mass transfer, as T evolves dynamically within the particle due to external heating and internal conduction.

The overall mass model is already integrated in *SPY* and Blondeau uses the following kinetic parameters in Equation 4.2 for the drying phase: $A_{moi} = 5.13\ 10^{10}$ s^{-1} and $E_{moi} = 88$ kJ mol^{-1}. In what concerns the volatile release, the parameters $A_{vol,i}$ and $E_{vol,i}$ in Equation 4.3 are species-dependent. These parameters are fitted to experimental data (TGA, DTG) for the specific biomass used. The exact values used in the simulation are reported in the work of Julien Blondeau [4].

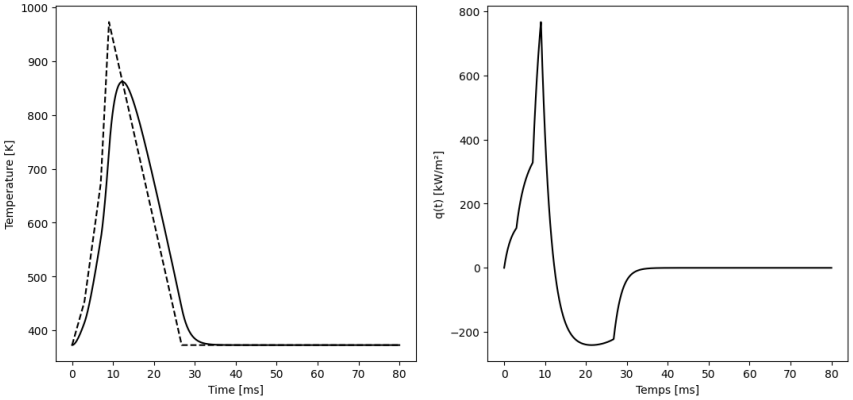

Figure 6: Engine-like dynamic heating (*biomass-fuelled*). (Left) Gas temperature (dashed) and Particle surface temperature (solid) vs. time for a particle radius of 20 μm, $h_{conv} = 3150\ Wm^{-2}K^{-1}$. (Right) Convective heat flux applied to the particle vs. time.

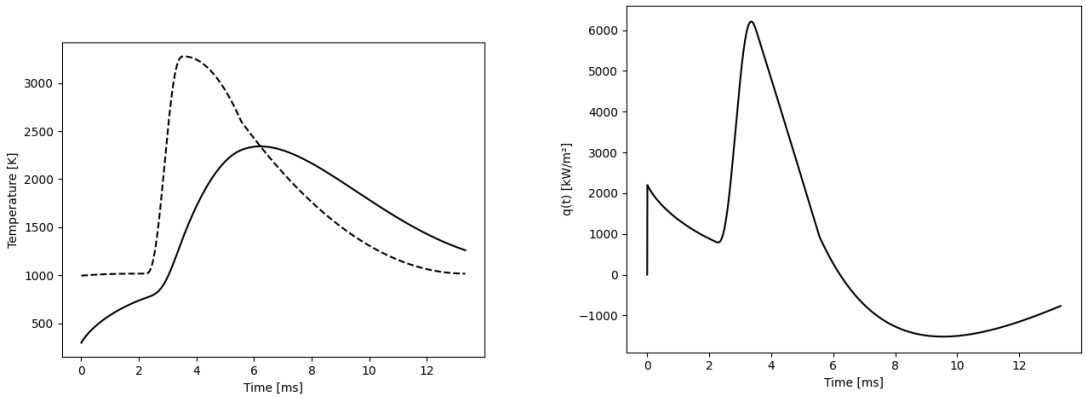

Figure 7: Engine-like dynamic heating (*diesel-fuelled*). (Left) Gas temperature (dashed) and Particle surface temperature (solid) vs. time for a particle radius of 20 μm, $h_{conv} = 3150\ Wm^{-2}K^{-1}$. (Right) Convective heat flux applied to the particle vs. time.

Part III
Char oxidation

6 Theoretical background

Following the pyrolysis reaction, a solid residue remains that must undergo combustion. This solid matrix, commonly referred to as fixed carbon or char, is primarily composed of carbon but can also be further decomposed and emits volatiles. The subsequent combustion process involving this residue in the presence of oxygen is known as char oxidation. The objective of this part is firstly to give a theoretical description of the phenomenon. In a second step, a model for the char oxidation reaction will be developed in order to estimate its mass loss rate for various particle sizes under various scenarios.

Char oxidation is a heterogeneous combustion and as it is a reaction of a gas (oxygen) with a solid (char), the process can be divided into the following processes:

1. Diffusion of the oxygen to the particle surface
2. Adsorption of the oxygen from the particle surface to an active site on the surface.
3. Desorption of the oxygen from the particle surface taking with it some atoms previously constituting the particle remaining content

The global oxidation rate is governed by two major controlling mechanisms:

- Mass transfer: oxygen diffusion to the surface, pore diffusion and product diffusion away from the particle surface
- Chemical kinetics: reaction rate depend on temperature and biomass characteristics

6.1 Oxidation regime and temperature zones

To be able to understand which step is controlling the reaction at specific condition, the relation of the particle reaction rate with temperature can be divided into three zones [5].

At low temperature, Zone I corresponds to a regime nearly only controlled by the third step mentioned above. It means that the oxygen is able to fully penetrate the particle surface and the reaction rate is then given by the chemical kinetic. At this stage, the temperature and the concentration are homogeneous within the particle. The mass loss is then characterised by the particle density decrease at constant volume. For small particles, the mass loss is characterised by the decrease of density even at high temperature [44].

Zone II corresponds to the intermediate-temperature regime, where the reaction rate is governed by a combination of chemical kinetics and diffusion: mixed control: the particle is thermally decomposed from both the outside and the inside. In this regime, the concentration of the reactive species near the particle surface is extremely low (close to zero) due to rapid consumption. The distance considered is typically shorter than the particle radius.

For high-temperature regime, corresponding to zone III, the reaction rate is controlled by the first step. In fact, the products form a layer around the particle limiting the mass transfer. The concentration of reactant species is small near the exterior surface of the particle. The mass transfer limits the rate: diffusion-controlled regime.

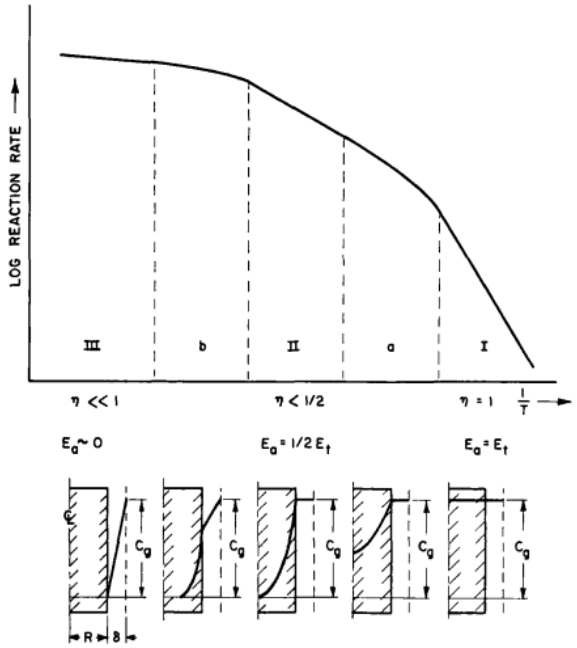

Figure 8: Variation of the reaction rate with the temperature [5]. This is a simplified graph, in practice it is not necessarily obeyed.

6.2 Oxygen diffusivity: temperature and pressure effects

In internal combustion engine, the fuel inside the chamber is subject to high pressure during the compression and ignition phase (more than 120 bar) [14]. The question about the influence of pressure on the reaction rate of char oxidation rises up. In order to characterise the degree of pressure influence, Charles R. Monson [45] has led coal char oxidation experiments at atmospheric and elevated pressure: from 1 atm to 15 atm total pressure. The sizes of the particles were about 40 μm and 70 μm, the same order of size of the particles studied in this work. In what concerns the pressures, the highest one is less than a quarter of the pressure obtained in combustion engine but the main goal here is to see the correlation between high pressure and reaction rate. The temperature inside the reactors varied between 1000 and 1500 K with low to atmospheric oxygen concentration. The authors used a classical nth-order kinetic equation in their global model to describe char oxidation:

$$r = k \cdot p_{O_2}^n \tag{6.1}$$

with r, the reaction rate, k, the rate constant, p_{O_2}, the oxygen partial pressure and n the reaction order. Here are the relevant results of the experiments:

1. Oxygen partial pressure increases reaction rate: when the total pressure remains constant but p_{O_2} increases, more O_2 reaches the reacting surface. This

leads to a faster chemical reaction rate because the reaction is kinetically controlled under these conditions.

2. Total pressure increase slows reaction: with p_{O_2} constant but higher total pressure, oxygen diffusivity decreases ($D_{O_2} \propto \frac{1}{P_{\text{tot}}}$). This results in less oxygen reaching the particle and thus a decrease in reaction rate. The combustion regime could shifts toward diffusion control.

In the case explained above, only the pressure has been taken into account, however, the in-cylinder elevated temperatures also need to be taken into account as it highly impacts the diffusivity. To illustrate this influence, an adapted equation from Bird (1960) and Welty (1984) is used:

$$D = D_0 \left(\frac{p_0}{p}\right) \left(\frac{T_g}{T_0}\right)^{1.5} \quad [m^2\ s^{-1}] \tag{6.2}$$

with D_0 [46] the diffusion coefficient of oxygen in carbon dioxide at 20 °C at 1 atm. The exponent in the temperature ratio highlights the strong sensitivity of oxygen diffusion to temperature variations. Nevertheless, the very high in-cylinder pressures typical of diesel engines exert an even greater influence, resulting in severely limited diffusion. Initially, a molecular collision factor is added in the equation. As the study covers only a single particle reaction, this factor is neglected.

6.3 Intrinsic kinetics

Intrinsic kinetics refers to the chemical reaction rate that are not influenced by any external physical transport phenomena but only by the temperature and the properties of the biomass. This true chemical behaviour of the reaction is controlled by several parameters:

- Activation energy E_i [J mol^{-1}]
- Pre-exponential factor A_i [s^{-1}]

The reaction rate follows the Arrhenius law:

$$k_i = A_i \cdot \exp\left(-\frac{E_i}{R_g\ T}\right) \tag{6.3}$$

where A_i and E_i values are defined either when adsorption or desorption is the limiting step. Desorption seems to be the limiting step for temperature around 1000-1650 K and the reaction is limited by adsorption when the temperature rises more than 1650 K [47].

In the context of char oxidation, the Langmuir-Hinshelwood mechanism is relevant for intermediate temperature, i.e where neither kinetics nor mass transfer fully dominates [48]:

$$k_{LH} = \frac{k_1 k_2 P_{O_2}}{k_2 + k_1 P_{O_2}} \tag{6.4}$$

k_{LH} the intrinsic reaction rate [mol $cm^{-3}\ atm^{-1}\ s^{-1}$] with k_1 refers to the adsorption reaction rate and k_2 the desorption reaction rate.

The adsorption/desorption mechanism, a two-step process, is crucial for understanding the temperature-dependent nature of surface-controlled reactions. At low temperatures, the surface is nearly saturated with adsorbed reactant, and the reaction rate becomes independent of gas-phase concentration. As temperature increases, desorption becomes more significant, reducing surface coverage and making the rate increasingly dependent on gas-phase reactant availability, leading to first-order behaviour. The determination of the reaction order n for carbon oxidation has been the subject of numerous research works. According to the work of H. E. Klimesh and R. H. Essenhigh [6], reported values typically range between 0.5 and 1, with the first-order reaction (n=1) generally considered the reference. In the present work, a first-order reaction is adopted, as no specific experimental determination was performed.

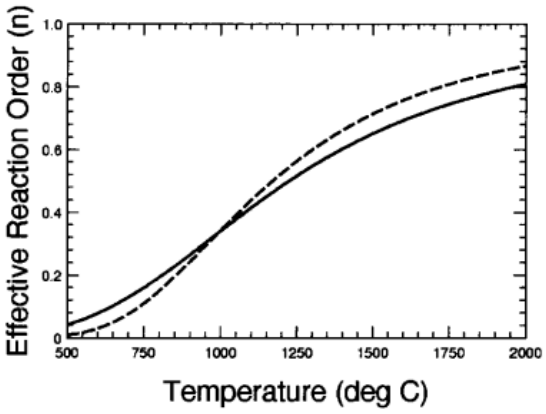

Figure 9: Variation of apparent reaction order with temperature derived from experimental data [6].

6.4 Global reaction rate formulation

As shown above, the oxidation rate is influenced by multiple factors such as the oxygen diffusion rate and the intrinsic chemical reaction rate. These factors are also highly influenced by pressure and temperature conditions. To account for all these elements in determining the particle's mass loss rate, directly linked to carbon consumption, a general expression can be formulated as follows [20]:

1. Firstly, the stoichiometric coefficient of carbon oxidation [kg C/kg O_2] is defined as:

$$v_c = \frac{12}{32} \cdot \frac{1 + \frac{M_{CO_2}}{M_{CO}} R_c}{1 + \frac{1}{2} \frac{M_{CO_2}}{M_{CO}} R_c} \tag{6.5}$$

   where R_c is the carbon ratio defined by Equation 6.14.

2. The diffusion kinetic coefficient is written:

$$K_d = Sh \cdot v_c \cdot \frac{D_{O_2}}{d_p} \frac{M_{O_2}}{R_g \, T_g} \tag{6.6}$$

   And the chemical kinetic corresponding to the adsorption limiting step:

$$K_c = A_c \cdot \exp\left(-\frac{E_c}{R_g \, T_p}\right) \tag{6.7}$$

Then K can be computed to define which of the two kinetic coefficients is the limiting one.:

$$K = \frac{1}{\frac{1}{K_d} + \frac{1}{K_c}} \tag{6.8}$$

3. The carbon consumption is then:

$$\frac{dC}{dt} = -\dot{m}_{O_2} \cdot v_c = -S_p K P_{O_{2,s}} \tag{6.9}$$

with

$$\dot{m}_{O_2} = \pi d_p Sh D_{O_2} \frac{M_{O_2}}{RT_g}(P_{O_{2,g}} - P_{O_{2,s}}) \tag{6.10}$$

The global reaction rate, representing the carbon thermal decomposition is then written as:

$$\frac{dC}{dt} = -S_p \frac{1}{\frac{1}{K_d} + \frac{1}{K_c}} P_{O_{2,s}} \tag{6.11}$$

with S_p, the external particle surface.

6.5 Reaction mechanisms and solid phase evolution

6.5.1 Carbon-Oxygen reaction pathways

Char oxidation starts once oxygen reaches the particle surface and starts reacting with carbon atoms. The following chemical equations show that carbon monoxide and carbon dioxide are both primary products of the oxidation of carbon [5]:

$$2C_f + O_2(g) \rightarrow 2C(O) \rightarrow 2CO(g) \tag{6.12}$$

$$C_f + O_2(g) \rightarrow C(O_2) \rightarrow CO_2(g) \tag{6.13}$$

C_f represents a carbon-free site and C(O) and $C(O_2)$ represent an atom of oxygen occupying a site.

The production of carbon monoxide and dioxide is temperature dependent. At low temperature, the ratio [CO/CO_2] is low (more carbon dioxide is emitted) and it increases with temperature. The relation between temperature and carbon production is illustrated with the following equation [49]:

$$R_c = \frac{[CO]}{[CO_2]} = 2500\ exp\left(\frac{-51843}{R_g T_p}\right) \tag{6.14}$$

6.5.2 Reactive surface recession and density loss

As the particle is subject to combustion, products are released causing its mass loss. This mass loss can be either due to the surface mass consumption or density loss. As explained in Subsection 6.1, in zone I, the particle density decreases at constant volume. In zone II, mass loss occurs within both processes: density loss and surface consumption. In the third regime, the mass loss is only characterized by a surface consumption that reduces the particle radius. With η the effectiveness factor which characterizes the oxygen penetration into the particle, two equations express the repartition of mass loss between the two phenomena:

$$dr = (1-\eta)\frac{dm}{4\pi r^2 \rho} \tag{6.15}$$

$$d\rho = \eta\frac{dm}{\frac{4}{3}\pi r^3} \tag{6.16}$$

$\eta = 1$ and $\eta = 0$ are the two limiting cases respectively for regime I and III.

The efficiency factor η, which ranges between 0 and 1, is defined as the ratio between the actual reaction rate and the rate that would exist in the absence of diffusion limitations. This efficiency results from the integration over the particle volume of the oxygen conservation equation, accounting for diffusion toward the centre and simultaneous consumption by chemical reaction. The authors in [50] show that:

$$\eta = \frac{3}{\phi}\left(\frac{1}{\tanh\phi} - \frac{1}{\phi}\right) \tag{6.17}$$

where the Thiele modulus ϕ is defined by:

$$\phi = \left(\frac{\beta \cdot k_{\mathrm{C,ox}} \cdot P_{O_2}^n \cdot S_V \cdot d_p^2}{D_{\mathrm{eff},O_2} \cdot M_{O_2}} \right)^{1/2} \tag{6.18}$$

with:

- β : mass stoichiometric coefficient $[kg_{O_2} kg_C{}^{-1}]$,
- D_{eff,O_2} : effective diffusivity of oxygen within the particle $[m^2\ s^{-1}]$,
- S_V : specific reactive surface area of the particle $[m^2 kg^{-1}]$,
- d_p : particle diameter [m],
- $k_{\mathrm{C,ox}}$: kinetic rate constant [kg $m^{-2} s^{-1} Pa^{-n}$)],
- P_{O_2} : oxygen partial pressure [Pa],
- n : reaction order.

6.5.3 Heat release

During its thermal decomposition, the particle is subject to heat due to convection with the surrounding gas but also due to the radiation with the chamber walls. The global heat balance is the following [20]:

$$C_p m_p \frac{dT_p}{dt} = h_p A_p (T_g - T_p) + A_p \varepsilon \sigma \left(T_w^4 - T_p^4 \right) - \frac{dW}{dt} H_w - \frac{dC}{dt} f_h H_C - \sum \dot{m}_i C_{p,i} T_i \tag{6.19}$$

The parameters of the gas in the equation are calculated for an average film temperature $\left(\frac{T_p + T_g}{2} \right)$ and the particle is treated as a gray body with constant emissivity ϵ. σ refers to the Stefan-Boltzmann's constant and is equal to $5.67 \cdot 10^{-8}$ $W\ m^{-2}\ K^{-4}$.

The term -$\frac{dC}{dt} f_h H_C$ refers to the exothermic contribution of char oxidation. As carbon consumption is associated with mass loss, adding a negative sign to the reaction rate term enables it to be treated as a positive heat contribution in the energy balance formulation. The factor f_h represents the heat release of char due to incomplete combustion.

$$f_h = 1 - 1.44 \cdot \left(1 - \frac{12}{32} \frac{1}{v_c} \right) \tag{6.20}$$

The term $\frac{12}{32} \frac{1}{v_c}$ represents the fraction of oxygen available per atom of carbon. If there is enough oxygen (large v_c), this fraction approach the stoichiometric value for complete oxidation to CO_2: f_h will be close to 1, meaning full heat release. Conversely, if oxygen is limited (small v_c), the term inside parentheses increases and thus f_h is smaller: heat release is reduced because more CO is produced instead of CO_2.

Terms that include the W subscript correspond to the drying step and the last term represents the heat fluxes supplied to the environment by the gases leaving the particle. In this equation, the contribution of heat by the gases entering the particle are not considered.

6.6 Ash production

After the oxidation, some inorganic material remains, which aggregates and collapses to form what is commonly referred to as ash. Biomass primarily consists of organic compounds (such as carbon, hydrogen and oxygen) and a smaller fraction of inorganic compounds including minerals and trace elements. During combustion, the organic matter is oxidized into gaseous products (CO, CO_2 and H_2O) whereas the inorganic fraction does not combust and instead remains as ash (see Figure 10). Ash formation occurs in several stages [51]:

1. Pyrolysis: volatile components are released, leaving behind a solid char containing both carbon and inorganic materials.

2. Char oxidation: as the carbon is consumed, the remaining non-combustible minerals accumulate and form solid ash particles.

3. Thermal transformations: some minerals undergo physical changes (e.g. melting, sintering, or volatilization), forming different ash types.

Following the work of V. Soloiu et al. [52], the presence of ash in biomass has a significant impact on diesel engine operation, primarily by accelerating wear and causing injector malfunctions. Even at relatively low levels (1-2%), ash contributes to abrasion of precision component such as injector needle, nozzle orifices and piston rings. This abrasive action increases the wear rate compared to a conventional diesel use, reducing the lifespan of the injectors and altering spray quality. Ash can also deposit on the injector tip and inside the nozzle leading to partial blockages which results in a deterioration of the combustion efficiency over time. Moreover, ash deposits promote sticking of the injector needle causing irregular engine performance and higher exhaust temperature. While measures such as reducing particle size, filtering and redesigning injectors with pressurized lubrication can mitigate some of these effects, the underlying abrasive nature of ash remains a limiting factor for long-term operation. Therefore, minimizing ash content (ideally below 1%) is crucial for maintaining engine reliability and sustaining performance when running on biomass-derived fuels.

In addition to its mechanical impact on engine components, ash can also influence combustion by modifying char oxidation kinetics, thereby affecting the rate and completeness of fuel conversion within the limited residence time of a diesel cycle. The presence or absence of ash alters both the availability and activity of surface sites. According to the study of R. Zhang et al. [53], many of these active sites are located at the crystallite edges of the char's porous structure, where defects and catalytic minerals promote oxygen access. If ash is removed, the associated catalytic minerals are largely eliminated, reducing the number of active sites and thereby slowing oxidation rates. This reduced reactivity can increase the residence time required for complete char burnout, which is critical in the short time available in an engine cycle. Conversely, the presence of certain ash components, such as alkali metals such as sodium, can have a catalytic effect, restoring surface reactivity and thus accelerating char conversion. However, in an engine environment, such catalytic benefits must be weighed against ash's abrasive and deposit-forming tendencies.

The influence of ash formation is not considered in this model as its integration would require additional parameters. The current parameters carry a certain degree of uncertainty so it might lead to reducing the model's accuracy.

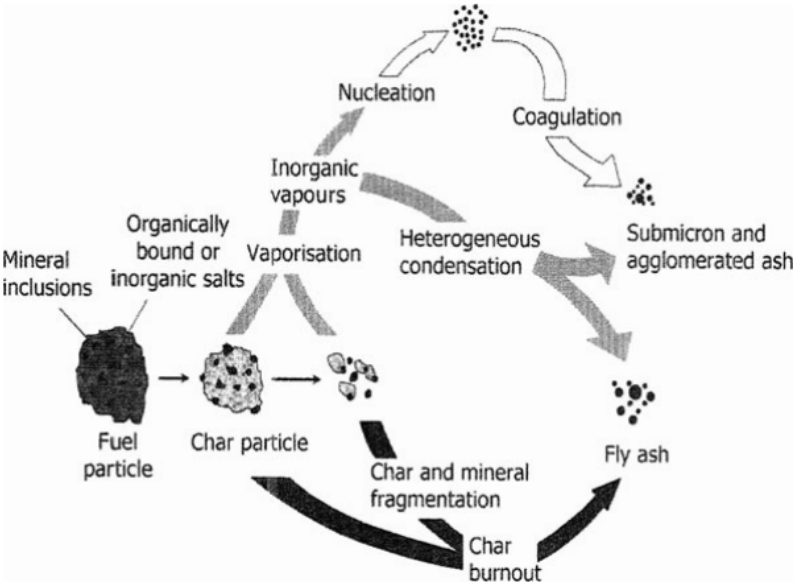

Figure 10: Physical transformations involved for ash formation during coal/biomass combustion [7]

Element	Org.-bound Elements	Minerals ionic	Salts
Na			$NaNO_3$, NaCl
K			KNO_3, KCl
Ca	Calcium pectate	Calcite , Calcium oxalate	$Ca(NO_3)_2$, $CaCl_2$
Mg	Chlorophyll, Magnesium pectate		$Mg(NO_3)_2$, $Mg(PO_3)_2$
S	Sulfolipids		SO_4^{2-}
N	Amino acids, proteins, Sulfolipids		
P	Nucleic acids	Phytates, Phytic acid	PO_4^{3-}
Cl			Cl^-
Al		Kaolinite	
Mn	Organic structures of proteins and carbohydrates		
Fe	Chelates	Phytoferritin	
	Organic sulfates	Iron oxide	

Table 5: Elemental forms in biomass: organic-bound elements, minerals, and ionic salts [10]

7 Numerical modelling of char oxidation

7.1 Particle geometry

The char oxidation is modelled using a 0D approach. The fixed carbon fraction is represented as a spherical particle with a density higher than that of the initial pine wood particle. Based on the work of C. E. Brewer et al. [54] and of J. Blondeau [4], the density of the fixed carbon is taken as approximately 2000 $kg\ m^{-3}$. The mass of carbon available for oxidation varies with the initial particle size. The particle volume for oxidation is calculated from the radius obtained after pyrolysis. Since *SPY* provides the temporal evolution of the particle surface area, the final radius at the end of pyrolysis can be directly extracted. It should be noted that the particle is assumed cylindrical in the pyrolysis model but spherical in the oxidation phase. As it is a 0D model, this geometric assumption mainly serves to evaluate the density decrease over time and to model the heating of the particle.

7.2 Heat transfer modelling

After the first phase of combustion, the particle starts to react with oxygen. Moreover, the surrounding temperature and in-cylinder pressure still vary with time and influence the oxidation rate. The initial particle temperature for the oxidation process is the temperature at which was the particle at the end of the pyrolysis process and it varies for each particle size. It varies depending on the initial radius and on the scenario. In what concerns the in-cylinder temperature (i.e. the gas temperature), the starting temperature is the temperature obtained at the time where the pyrolysis is assumed finished. It is also important to remind that the particle is considered thermally thin due to its very small size (r $<$ 50 μm). The internal thermal resistance is negligible. As a result, no significant temperature gradient develops within the particle, and its temperature can be considered spatially uniform at any given time. Once subject to the combustion environment, the particle is exposed to heat [20]:

- By convection with the surrounding gas
- By radiation with the internal wall of the combustion chamber

The gas temperature is imposed following the same profiles as for the pyrolysis (see Subsubsection 5.2.3). At each time step, the heat transfer rate into the particle is computed using a lumped-capacity model, meaning the particle is assumed to have a uniform internal temperature (no internal thermal gradient). The governing equation is:

$$\frac{dT_p(t_i)}{dt} = -\frac{h_{conv} \cdot A_{ext}}{\rho_p \cdot V \cdot c_{p,char}}(T_p(t_i) - T_g) \tag{7.1}$$

With h_{conv}, the equivalent convective heat transfer coefficient computed before for the pyrolysis boundary conditions implementation and the char heat capacity $c_{p,char}$ from Blondeau [4]:

$$c_{p,char} = 1430 + 0.355T - 7.32 \cdot 10^7 T^{-2} \tag{7.2}$$

The heat balance results in a gradual temperature variation of the particle over time numerically integrated using Euler's explicit method. The particle temperature T_p(t)

evolves as:

$$T_p(t_i) = max(T_p(t_{i-1}) + \frac{dT}{dt} \cdot t_i,\ T_{min}) \tag{7.3}$$

This formulation accounts solely for convective heat exchange between the particle and the surrounding gas, excluding other mechanisms such as radiative heat transfer or internal conduction within the particle. Consequently:

- Once the in-cylinder gas temperature reaches its peak and begins to decrease, the particle temperature also declines. This cooling is governed by the convective heat transfer rate and follows the same dynamics as the heating phase.
- Since the carbon oxidation rate is strongly temperature-dependent (Arrhenius law), the heat transfer directly influences the combustion kinetics. The duration of the oxidation process therefore depends on both the magnitude and the rate of temperature variation.

The oxidation model scenarios are the continuity of the three scenarios previously detailed in the pyrolysis modelling section (Section 5).

7.3 Mass and density loss

C. Guillaume [44] showed that, at high temperature and for small radii, mass can be removed either by a uniform density decrease or by surface regression (i.e. Zone I and Zone II regimes). In this study only the Zone I regime is considered: the char particle is oxidized throughout its volume, so that solid carbon is consumed uniformly; the particle volume remains constant while its density and mass decrease over time. The governing equation for mass loss is:

$$\frac{d\rho_c}{dt} = -\left(\frac{dC}{dt}\right)\frac{1}{V_p}\ \ [kg\ m^{-3}\ s^{-1}] \tag{7.4}$$

where ρ_c is the char particle density and V_p is the spherical constant volume.

The rate of carbon consumption is calculated by combining the chemical reaction rate and the diffusion in series as depicted by Equation 6.11. This formulation assumes that the reaction may be limited either by chemical kinetics or by oxygen diffusion around the particle depending on the in-cylinder conditions. By expressing the overall rate as a series combination, the slower of the two processes exerts a greater control over the total reaction rate

7.4 Intrinsic kinetics and diffusion parameters

Some of the equations presented above require parameters that are typically determined from experimental data. This is the case for the intrinsic kinetic parameters A_i (intrinsic pre-exponential factor, $[s^{-1}]$) and E_i (intrinsic activation energy, $[\text{J}\cdot\text{mol}^{-1}]$). These parameters are challenging to estimate without dedicated measurements. A common approach is to fit them to experimental data obtained under similar operating conditions. Based on literature values [55, 56] and, more specifically, the work of Toporov [8], suitable kinetic parameters were identified, enabling the modelled curve to closely match the experimental results, as shown in Figure 11. The resulting parameters, subject to some degree of uncertainty, are:

- $E_i = 160 \cdot 10^3$ $[\text{J}\cdot\text{mol}^{-1}]$
- $A_i = 7.2 \cdot 10^3$ $[s^{-1}]$

These same parameters are applied in the char oxidation model for all scenarios, despite the conditions variations. Although this assumption may reduce accuracy in the absence of dedicated experimental data, the model still provides relevant estimates for oxidation durations.

In addition to chemical kinetics, the oxidation rate is influenced by oxygen diffusion from the bulk gas to the particle surface. As illustrated in Equation 6.2, the diffusion coefficient is expressed as a function of both pressure and temperature to reflect in-cylinder conditions [9, 14] with the reference oxygen thermal diffusivity coefficient $D_0 = 22.39 \cdot 10^{-6}$ $m^2 s^{-1}$.

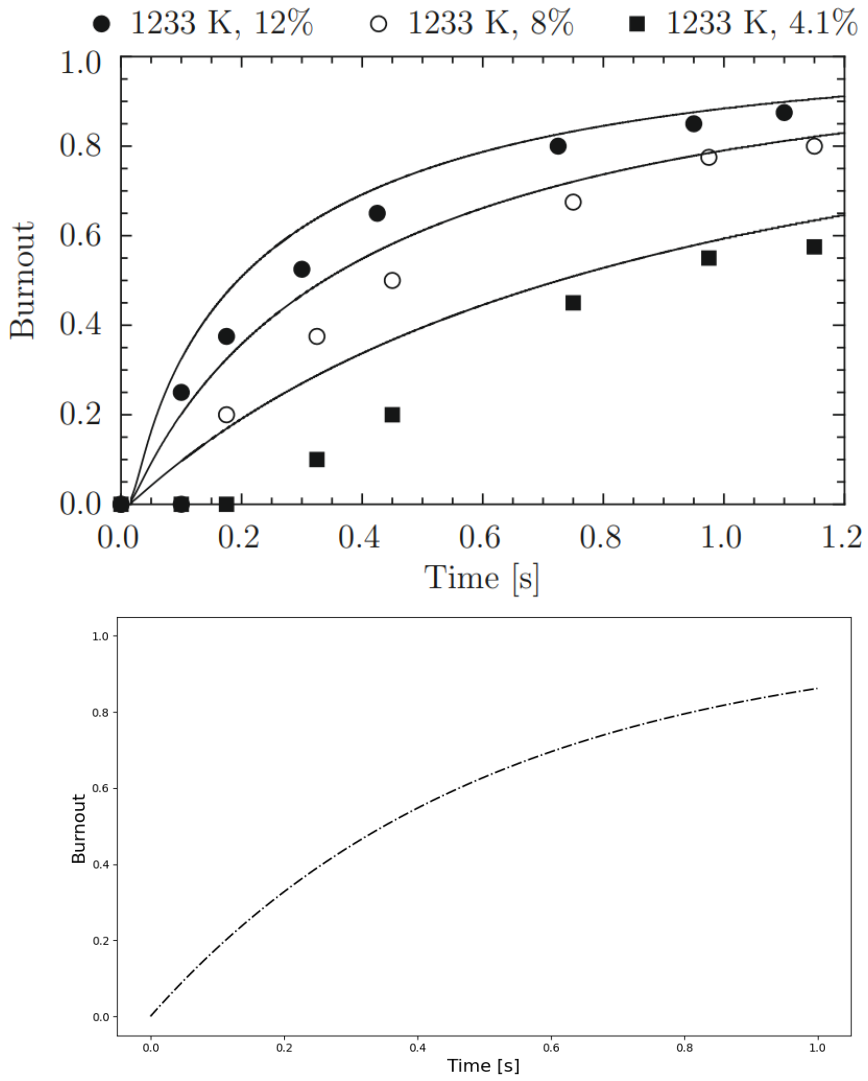

Figure 11: (Top) Work from Toporov [8] on char particles, $d = 80$ μm. Experimental (discrete points) and calculated (curves) mass release vs. time at high temperature and with different models [8]. (Bottom) Char oxidation model for a biomass particle, $d = 80$ μm at constant temperature T = 1273 K.

7.5 Char oxidation initial parameters

Based on the previously introduced assumptions and governing equations, it is now possible to simulate the oxidation of char of a single pine wood particle. As shown Part II, the pyrolysis duration can be identified from thermal and mass evolution data. This information allows to extract data such as the residual mass, the particle temperature and the particle surface at the end of the pyrolysis, corresponding to the start of the second combustion phase. These data serve as the initial conditions for the char oxidation. A consolidated overview of these key parameters is provided in Subsection 8.1 and in Subsection 8.2.

In the oxidation model, the particle is assumed to retain a constant geometric volume while its density decreases due to carbon consumption. This contrasts with the pyrolysis phase, during which the particle cylindrical volume evolves. To define the char oxidation starting volume, new radii must be computed based on the residual particle surface S_{res} after pyrolysis.

$$r_{\text{char}} = \left(\frac{S_{\text{res}}}{6\pi} \right)^{\frac{1}{2}} \tag{7.5}$$

The resulting radius r_{char} defines the particle geometry for the oxidation phase, which is then kept constant throughout the simulation while the density evolves (see Subsection 7.3):

$$V_{\text{char}} = \frac{4}{3}\pi r_{char}^3 \tag{7.6}$$

Part IV
Global analysis and perspectives

8 Total conversion time: pyrolysis and oxidation

This section presents and analyses the total combustion duration of a pine wood particle under different in-cylinder conditions. Since the end of the pyrolysis process is arbitrary (being potentially prolonged if a heat source continues to raise or maintains the particle's temperature high enough), it is defined here numerically. Specifically, the end of pyrolysis is set at the moment when the slope of the relative mass loss rate curve flattens, indicating that further mass loss becomes negligible or null. At that point, key data are extracted: the bulk gas temperature, the particle temperature, the remaining mass fraction and the particle surface. These values are then used as initial conditions for the char oxidation phase. The duration for the oxidation phase is the time required for the particle mass to decrease down to 0.

The particle, which is initially at 298 K with a moisture content of 8%, is injected into the combustion chamber at t=0. For the pyrolysis model the reference time t_0 is defined at the moment of injection, which approximately occurs at 21.5 CAD before Top Dead Centre (TDC) [9]. For the char oxidation, the t_0 refers to the chosen end of the pyrolysis process.

The total combustion duration corresponds to the sum of the elapsed times for the two phases. It is worth noting that, in diesel engines, combustion typically needs to be completed within less than 60 crank angle degrees (CAD) after injection [15]. For reference, at 1500 rpm, a rotation of 60° corresponds to approximately 6.66 ms.

The following scenarios aim to best represent the in-cylinder conditions of a diesel engine. In the first case, experimental data from Stover et al. [14] is used to model the in-cylinder temperature profile at 1500 rpm. In this experiment, the fuel used is biomass, and the recorded temperatures are relatively low. Simulations based on this temperature profile result in incomplete pyrolysis by the end of the engine cycle. To better replicate the conditions inside a compression engine, additional temperature profiles were developed using data from U. Rajak & T. Verma [9] and from a SAE paperwork [43]. These updated profiles feature higher in-cylinder temperatures and pressures, which were then applied for the combustion simulation.

Results are organized as follows: for each initial radius, we first report the pyrolysis data, followed by the char oxidation data. For clarity, the reported "oxidation radius" is the initial particle radius (i.e., before pyrolysis), not the actual initial radius for the oxidation phase. The approximate radii actually used in the combustion model are listed in the table below for reference (depending on the scenario, these radii may differ by ±2%).

Radii before pyrolysis [μm]	10	12	15	20	30	50	75	100
	↓	↓	↓	↓	↓	↓	↓	↓
Radii after pyrolysis [μm]	7.16	9.28	11.62	14.36	21.58	36	53.92	72.92

Table 6: Particle radii before and after pyrolysis.

8.1 Biomass-fuelled engine temperature profile

In this case, the pyrolysis process terminates at a clearly defined moment, specifically when the bulk gas temperature starts to decrease. The residual mass fraction is directly influenced by this temperature drop. As shown in Figure 12a, small particles heat up quickly and experience significant mass loss within a short time window. In contrast, thicker particles display a much lower mass loss (around 10%), due to their slower thermal response. For these larger particles, the release of volatiles is strongly hindered by lower surface temperatures (around 600 K). In this scenario, only the drying phase is effectively completed for the largest particles.

Regarding fixed carbon degradation, the rapid bulk gas temperature decrease during the expansion phase limits the heat transfer required to sustain carbon oxidation. As a consequence, fixed carbon conversion is severely restricted, resulting in a high residual carbon content by the end of decompression that must then be expelled.

In this scenario, the particle surface temperature closely follows the bulk gas temperature profile when the particle diameter is small enough (see Figure 12c). As explained above, the convective heat coefficient is inversely proportional to the particle's radius. Large particles take too long to heat up leading to an insufficient particle's temperature to initiate pyrolysis and char oxidation. Numerical results indicate that the residual mass is about 90% of the initial mass: pyrolysis is highly incomplete in these cases. Using oversized biomass particles in a diesel engine can have several detrimental effects: their greater thermal inertia prolongs both pyrolysis and char oxidation, often exceeding the available residence time in the combustion chamber. This leads to incomplete combustion and the deposits accumulation on engine walls and components accelerates the wear of the cylinder. Moreover, the delayed or incomplete release of volatiles can disrupt combustion timing and homogeneity, potentially causing localized hot spots or even knocking. Such factors degrade engine performance and may accelerate wear or damage to critical components. To conclude, when the surrounding temperature is insufficient, pyrolysis cannot be complete, even for the smallest particles and the char oxidation cannot start. This highlights the strong dependence of the process on thermal conditions.

	Radius [μm]	t_{end} [ms]	$T_{\text{p,start}}$ [K]	$T_{\text{p,end}}$ [K]	Initial mass [kg]	m_{res}/m_0 [%]
Pyrolysis	10	10.38	298	935.97	0.0025e-10	31.14
	12	11.07	298	918.78	0.0044e-10	31.25
	15	12.64	298	881.18	0.0085e-10	32.12
	20	17.60	298	757.66	0.0201e-10	43.13
	50	18.50	298	632.81	0.3147e-10	89.77
Char oxidation*	10	8.50	935.97	678.75	0.078e-12	99.33
	12	8.50	918.78	674.16	0.130e-12	99.55
	15	8.10	881.18	666.50	0.270e-12	99.77
	20	7.10	797.01	648.83	0.870e-12	99.99
	50	/	630.56	/	0.282e-10	100.00

Table 7: Numerical results under biomass-fuelled engine-like dynamic heating scenario.
*The radius is shown here for clarification; in reality, it differs between the pyrolysis and oxidation phases.

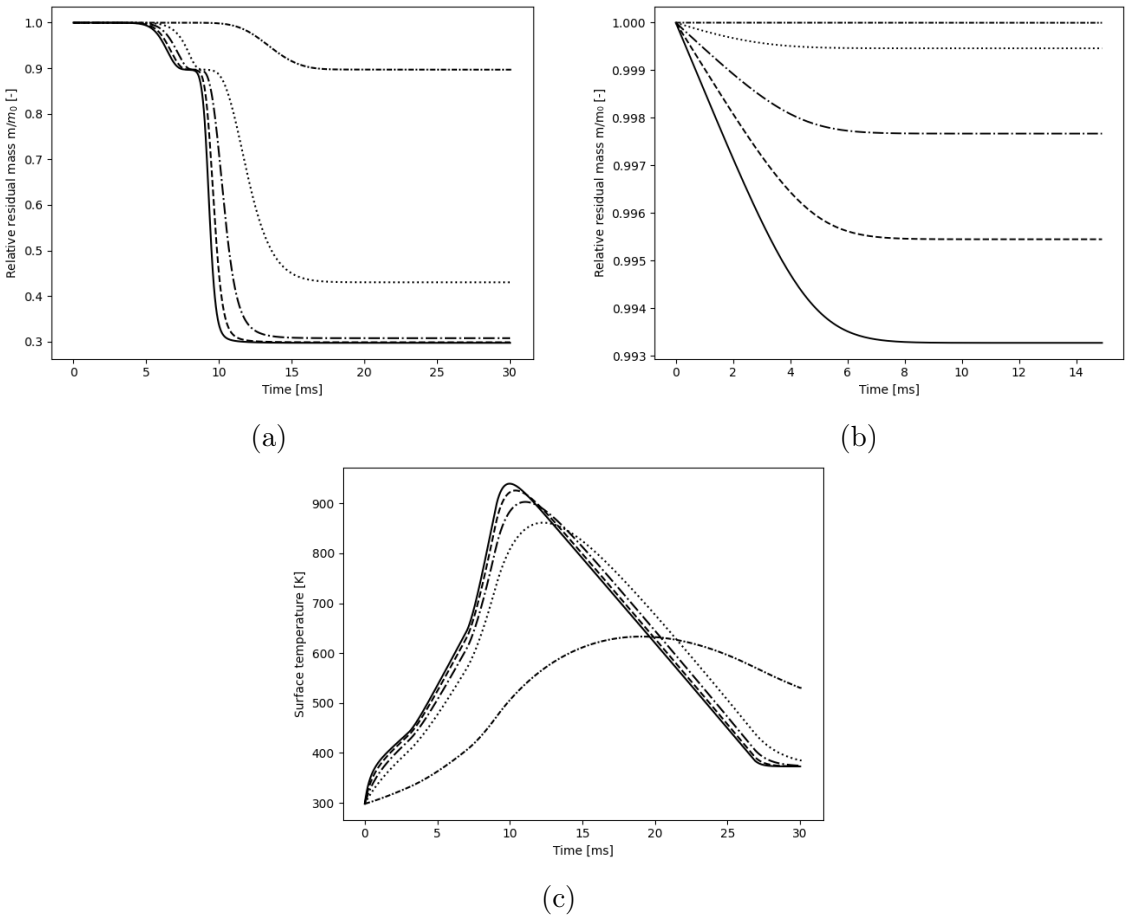

Figure 12: Graphs for the engine-like scenario for five different pine wood particle radii: 10 μm (solid), 12 μm (dashed), 15 μm (dashdot), 20 μm (dotted) and 50 μm (shorter dashdot). (a) Pyrolysis computed with SPY. (b) Oxidation of the remaining fixed carbon content. (c) Temperature profiles.

8.2 Diesel-fuelled engine temperature profile

These numerical experiments simulate the thermal conversion of pine wood microparticles under diesel-fuelled compression engine conditions. The technical specifications of the reference engine are given in Table 16 in Appendix B. Three different temperature profiles (see Figure 16) are considered, each tested for various particle sizes. The particle is injected into a hot environment and subjected to convective heat transfer. The pyrolysis duration is determined, as in previous sections, by the point at which the mass flux drops to zero.

Table 9 presents the numerical results for both pyrolysis and char oxidation under the different temperature scenarios. Since no specific data for the 1000 rpm engine speed was available in the study by Rajak and Verma [9], the required values were extrapolated from known points. The pyrolysis simulation window starts from the particle injection into the hot environment until no more mass loss is detected. The TDC position occurs 21.5 CAD after injection, coinciding with the maximum in-cylinder temperature and pressure. The in-cylinder pressure rises from atmospheric to 154 bar [9]. The maximum pressure difference observed between the different scenarios was negligible (approximately 4 bar). Therefore, for simplicity, the same pressure profile (see Figure 17 in Appendix B) was applied to the char oxidation stage in all scenarios. The extremely high in-cylinder pressure results in very low oxygen diffusivity, making the oxidation process entirely diffusion-controlled: the intrinsic kinetic parameters previously defined no longer influence the reaction rate.

A first observation is that particles with a radius larger than 50 μm are too thick to complete pyrolysis within the available time window (120 CAD), which is bounded by the injection event and the end of the expansion phase. As engine speed increases, in-cylinder peak temperatures and pressures also rise, leading to faster pyrolysis of the small particles but not for the larger ones. In fact, larger particles require more time to heat up compared to smaller ones due to their lower surface-to-volume ratio: the convective heat transfer coefficient is directly influenced by particle size [42].

The oxidation times reported correspond to the theoretical time required for complete conversion (m_{res}=0). For the oxidation temperature profiles, the available data cover only the combustion and exhaust phases, with a minimum temperature of about 1017 K that remains constant over time. This limitation does not affect the interpretation of the results: if a particle reaches this minimum temperature, it is already too late for it to be considered a viable working size. For example, a particle with a radius of 50 μm requires roughly 125 ms to complete both pyrolysis and oxidation, whereas the total combustion in a diesel engine must occur within about 60 CAD, corresponding to 10 ms at 1000 rpm. Even with this artificially high minimum temperature (which underestimates the actual oxidation time due to the strong temperature dependence of the reaction rate), the total reaction time remains far too long.

On Figure 13a, Figure 14a and Figure 15a, the distinction between thermally thin and thermally thick particles becomes more pronounced as the engine speed increases and the particles are exposed to higher temperatures but within a shorter time. For small particles (particularly those with radii of 20 and 30 μm), the mass loss curves tend to converge, giving shorter pyrolysis durations. In contrast, larger particles (with radii above 50 μm) also show convergence, but towards a residual mass fraction close to 1, reflecting incomplete conversion. Interestingly, at lower temperatures (with peaks still reaching 2600 K) and slower engine speeds, large particles undergo more extensive pyrolysis than at higher temperatures, due to the longer time window available for the process. For a 60 CAD combustion window, the corresponding durations are 10 ms at 1000 rpm, 8.33 ms at 1200 rpm and 6.66 ms at 1500 rpm.

As a preliminary conclusion, particles with a radius greater than 50 μm exhibit total combustion durations that largely exceed the 60 CAD limit, with their pyrolysis phase alone already surpassing the available time. For particles with a radius below 50 μm, the pyrolysis duration fits within the time window; however, their complete oxidation still exceeds the limit by several milliseconds. In Table 8, the combustion of a 10 μm radius particle is simulated under the three previously described scenarios. For this particle size, complete combustion occurs within 60 CAD, suggesting it could be suitable for use in a diesel engine. For this particle size, the corresponding graphs are not shown, as they do not provide any additional visual information compared to the cases already presented for the other particles.

	Radius [μm]	Engine speed [rpm]	t_{end} [ms]	$T_{\text{p,start}}$ [K]	$T_{\text{p,end}}$ [K]	Initial mass [kg]	m_{res}/m_0 [%]
Pyrolysis	10	1000	6.09	298	2532	0.0025e-10	5.42
	10	1200	5.11	298	2711.33	0.0025e-10	5.41
	10	1500	4.01	298	2886.23	0.0025e-10	5.37
Char oxidation*	10	1000	2.65	2532	2426	0.0135e-12	0.0
	10	1200	2.69	2711	2443	0.0135e-12	0.0
	10	1500	2.64	2886	2482	0.0135e-12	0.0

Table 8: 10 μm radius particle combustion numerical results for diesel-fuelled engine-like dynamic heating scenario at 1000, 1200 and 1500 rpm engine speed.
*The radius is shown here for clarification; in reality, it differs between the pyrolysis and oxidation phases.

1000 rpm	Radius [μm]	t_{end} [ms]	$T_{\text{p,start}}$ [K]	$T_{\text{p,end}}$ [K]	Initial mass [kg]	m_{res}/m_0 [%]
Pyrolysis	20	6.57	298	1937.12	0.0201e-10	6.07
	30	7.31	298	1511.76	0.0680e-10	8.46
	50	16.54	298	1195.47	0.3147e-10	9.33
	75	108.80	298	1006.89	1.0622e-10	10.66
	100	201.20	298	1001.37	2.5171e-10	9.87
Char oxidation*	20	13.28	1937.12	1385.0	0.122e-12	0.0
	30	35.14	1511.76	1086.4	0.575e-12	0.0
	50	111.10	1195.47	1023.4	2.936e-12	0.0
	75	256.08	1006.89	1017	11.32e-12	0.0
	100	454.20	1001.37	1017	24.84e-12	0.0
1200 rpm	Radius [μm]	t_{end} [ms]	$T_{\text{p,start}}$ [K]	$T_{\text{p,end}}$ [K]	Initial mass [kg]	m_{res}/m_0 [%]
Pyrolysis	20	5.41	298	1924.13	0.0201e-10	6.2
	30	6.33	298	1527.9	0.0680e-10	8.45
	50	16.04	298	1163.93	0.3147e-10	9.62
	75	116.30	298	1008.09	1.0622e-10	10.33
	100	202.50	298	1001.38	2.5171e-10	9.87
Char oxidation*	20	13.73	1924.13	1290.8	0.1246e-12	0.0
	30	35.95	1527.9	1072.6	0.575e-12	0.0
	50	111.70	1163.93	1022	3.027e-12	0.0
	75	256.0	1008.09	1017	10.97e-12	0.0
	100	454.17	1001.38	1017	24.84e-12	0.0
1500 rpm	Radius [μm]	t_{end} [ms]	$T_{\text{p,start}}$ [K]	$T_{\text{p,end}}$ [K]	Initial mass [kg]	m_{res}/m_0 [%]
Pyrolysis	20	4.44	298	1965.16	0.0201e-10	6.19
	30	5.41	298	1558.9	0.0680e-10	8.35
	50	13.39	298	1140.64	0.3147e-10	12.51
	75	123.60	298	1009.17	1.0622e-10	10.09
	100	203.70	298	1001.38	2.5171e-10	9.87
Char oxidation*	20	14.28	1965.16	1214.1	0.124e-12	0.0
	30	36.62	1558.9	1062.2	0.0680e-12	0.0
	50	112.01	1140.68	1021.2	3.936e-12	0.0
	75	255.87	1009.17	1017	10.72e-12	0.0
	100	454.15	1001.38	1017	24.84e-12	0.0

Table 9: Numerical results: pine wood particle combustion under diesel-fuelled engine-like dynamic heating scenario at 1000, 1200 and 1500 rpm engine speed.
*The radius is shown here for clarification; in reality, it differs between the pyrolysis and oxidation phases.

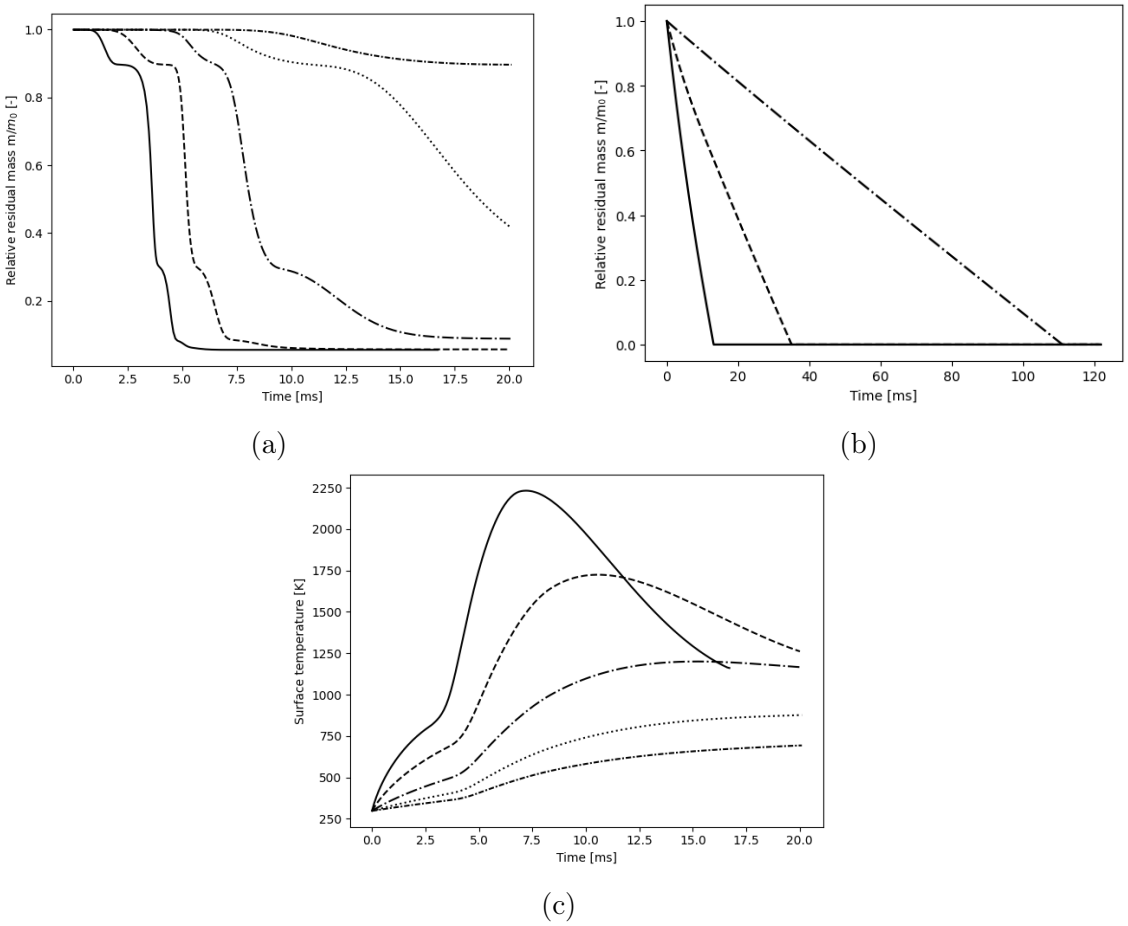

Figure 13: Graphs for the diesel-fuelled engine-like conditions at 1000 rpm for five different pine wood particle radii: 20 μm (solid), 30 μm (dashed), 50 μm (dashdot), 75 μm (dotted) and 100 μm (shorter dashdot). (a) Pyrolysis computed with SPY. (b) Oxidation of the remaining fixed carbon content (for clarity, only the three smallest particle sizes are shown). (c) Temperature profiles.

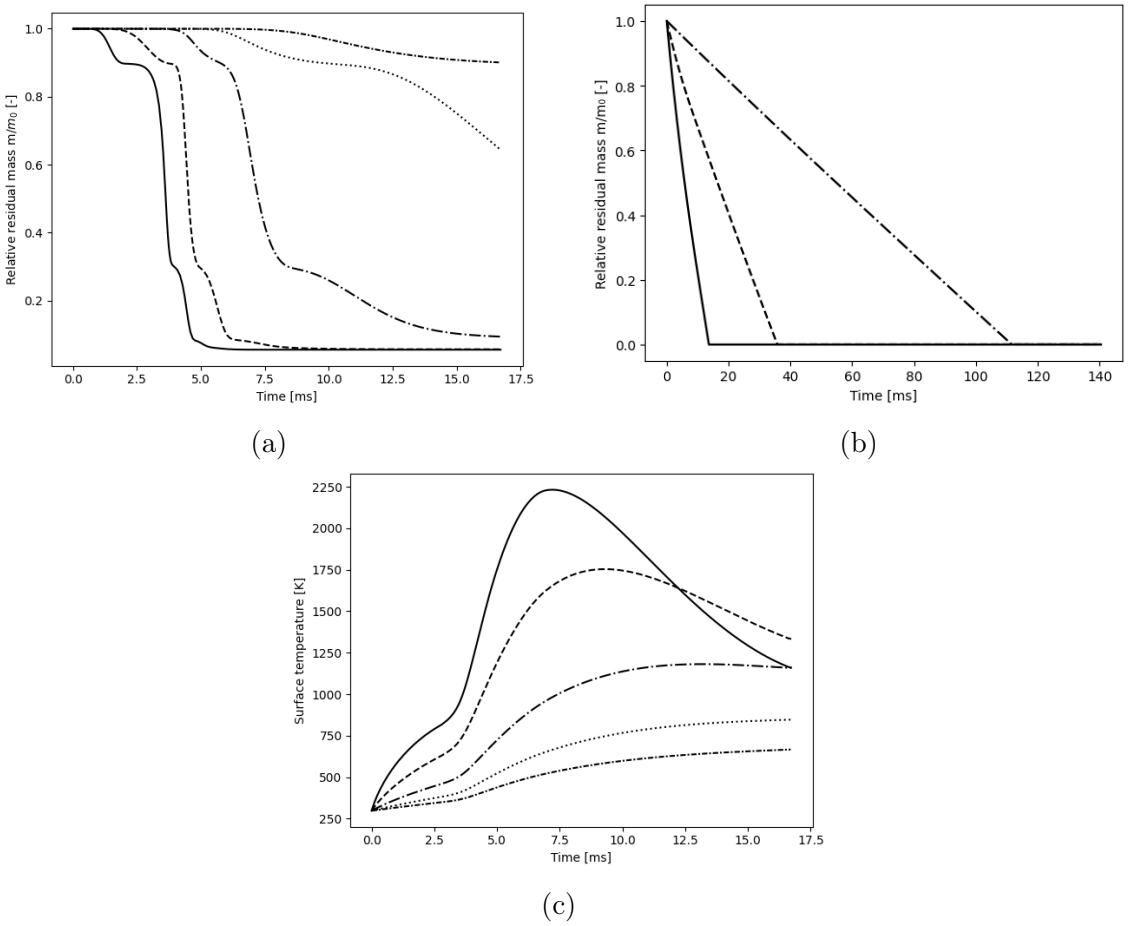

Figure 14: Graphs for the diesel-fuelled engine-like conditions at 1200 rpm for five different pine wood particle radii: 20 μm (solid), 30 μm (dashed), 50 μm (dashdot), 75 μm (dotted) and 100 μm (shorter dashdot). (a) Pyrolysis computed with SPY. (b) Oxidation of the remaining fixed carbon content (for clarity, only the three smallest particle sizes are shown). (c) Temperature profiles.

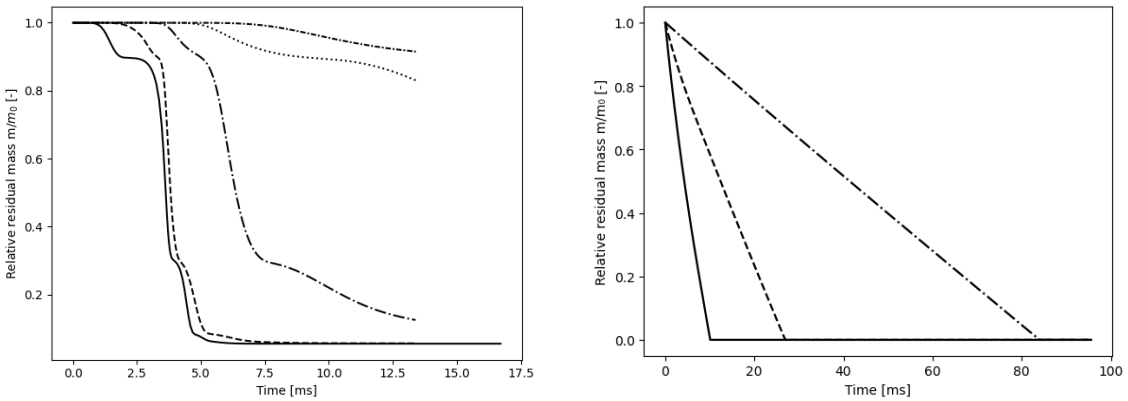

(a) (b)

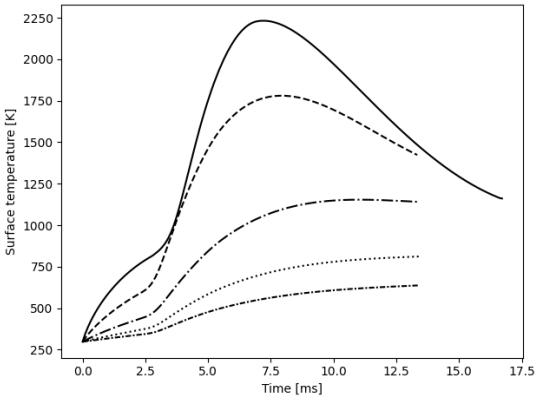

(c)

Figure 15: Graphs for the diesel-fuelled engine-like conditions at 1500 rpm for five different pine wood particle radii: 20 μm (solid), 30 μm (dashed), 50 μm (dashdot), 75 μm (dotted) and 100 μm (shorter dashdot). (a) Pyrolysis computed with SPY. (b) Oxidation of the remaining fixed carbon content (for clarity, only the three smallest particle sizes are shown). (c) Temperature profile

8.3 Limitations and perspectives

The in-cylinder conditions used for these numerical experiments were obtained from experimental studies [9, 14, 43]. While the values were transcribed as accurately as possible, some uncertainties inevitably remain. Temperature profiles around the injection phase may exhibit minor discrepancies between the literature data and the implemented script; however, the overall curve shape is preserved and the peak values match the experimental data. For the diesel-fuelled scenario, the minimum in-cylinder temperature is about 1017 K but in reality the temperature drops during the expansion phase to a much lower value, approximately 300 K [57]. Without maintaining high and constant temperature after the expansion phase, it would have been impossible to start the oxidation phase, at least for the bigger particles. Furthermore, since mass loss is directly associated with density reduction, density becomes a key parameter to consider. Reported values for char density vary across studies; in this work, the upper bound was selected (i.e. 2000 $kg\ m^{-3}$) to maximise the overall combustion duration, thereby allowing the limiting case to be observed even at high density.

It is important to note that combustion is an inherently complex process, involving volatile interactions, radiative heating from cylinder walls, particle–particle interactions in the case of powder combustion, and heat release from thermal degradation. In reality, in-cylinder temperature is not spatially uniform. Localized hot spots [58] can occur during the cycle, creating significant temperature gradients between regions. Regarding particle temperature, although the particle is assumed to be thermally thin, there remains a significant difference between the local particle temperature and the global in-cylinder temperature. In this study, the global in-cylinder conditions are imposed, while the local particle temperature is computed numerically. As a result, the predicted particle temperature is lower than the bulk gas temperature, since heating occurs only via a convective exchange between the two. Including additional heat transfer mechanisms would require a more detailed model, which would add complexity and potentially introduce further uncertainties into the computation.

From a perspective of future improvements, several parameters could be refined. The maximum in-cylinder temperature observed when using biomass [14] as fuel is significantly lower than that obtained with diesel [9, 43]. In this study, the temperatures applied are therefore either too low or considerably higher than what would realistically occur with biomass combustion. More accurate experimental data from biomass-fuelled engines is needed to ensure realistic modelling. Moreover, in reality, pyrolysis and char oxidation are not sequential but overlapping processes. In the present work, the total duration is calculated as if the second phase begins only after the first has ended. A more advanced model should be developed to account for this overlap, allowing a more accurate prediction of conversion times and residual mass fractions.

Additional improvements could also include:

- Incorporating radiative heat transfer from the cylinder walls and from surrounding particles, which can have a significant impact on particle heating rates.
- Using biomass particles with less moisture content.

- Accounting for spatial temperature and pressure gradients within the combustion chamber, including the presence of hot spots, which may enhance or limit local reaction rates.
- Modelling particle–particle interactions
- Using a CFD approach to simulate the in-cylinder non-homogeneous temperature fields.
- Conducting an emissions analysis to assess the potential benefits of using biomass over fossil fuels such as diesel.

Such refinements would allow for a more realistic model, improving the understanding and optimisation of biomass particle combustion in diesel engine environments.

8.4 Conclusion

This work aims to simulate the thermal behaviour and mass conversion of a single particle under internal combustion engine (ICE) conditions, more specifically diesel engine. Particle's drying and pyrolysis phases were simulated thanks to an already developed model called SPY [4]. For the char oxidation, a simplified model was implemented accounting the pressure and temperature influence on oxygen diffusivity.

The results highlight key trends consistent with the literature: the influence of particle size on thermal inertia and the contribution to volatile release and char oxidation to the overall mass loss. The models capture the general thermal response of a particle in a high-speed heating and cooling environment and under high pressure. The current approach offers a useful framework for studying biomass particle in ICE conditions but the assumptions made inevitably lead to deviations from experimental trends. However, small particles with radii below 50 μm generally complete pyrolysis within the time available in a typical diesel cycle ($<$ 60 CAD), but their full oxidation often exceeds this window. Only the smallest particles tested, with radii equal to 10 μm, achieve complete combustion within the allocated time. These results suggest that very fine particles are better suited for use in compression engines. It is expected that higher in-cylinder temperatures would accelerate conversion rates, thereby enabling larger particles to combust fully within the 60 CAD window. Conversely, the reduced oxygen diffusivity associated with high pressures acts as a limiting factor, slowing conversion. At lower pressures, the enhanced diffusivity would make the process more strongly controlled by chemical kinetics leading to faster conversion rates.

Appendix

A Proximate and ultimate analysis and structural composition of biomass sample

Table 10: Proximate analysis of selected biomass samples [11].

Sample	**MC (%)**	**VM (%)**	**FC (%)**	**Ash (%)**	**pH**
Siam weed	1.12 ± 0.04	78.11 ± 0.7	15.87 ± 0.04	4.90 ± 0.02	12.50
Gmelina arborea	2.19 ± 0.02	84.61 ± 0.8	11.14 ± 0.05	2.06 ± 0.01	10.67
Sugarcane straw	0.90 ± 0.04	77.25 ± 0.4	13.31 ± 0.06	9.60 ± 0.01	10.46
Rice husk	0.89 ± 0.05	61.80 ± 0.6	16.44 ± 0.03	20.89 ± 0.02	11.14
Shea butter wood	0.18 ± 0.03	85.20 ± 0.7	13.68 ± 0.07	0.94 ± 0.01	9.98
Palm kernel shell	0.40 ± 0.02	73.70 ± 0.6	22.40 ± 0.05	3.50 ± 0.01	10.39
Bamboo wood	1.03 ± 0.05	80.20 ± 0.1	14.13 ± 0.08	4.64 ± 0.02	11.45

MC: Moisture content; **VM**: Volatile matter; **FC**: Fixed carbon.

Table 11: Ultimate analysis of selected biomass samples [11].

Sample	**C (%)**	**H (%)**	**N (%)**	**O (%)**	**S (%)**	**HHV**	**LHV**
Siam weed	45.82 ± 0.3	5.79 ± 0.03	1.20 ± 0.01	46.95 ± 0.2	0.24 ± 0.03	20.40	19.14
Gmelina arborea	47.50 ± 0.1	5.65 ± 0.03	0.27 ± 0.02	46.42 ± 0.1	0.16 ± 0.01	19.15	17.92
Sugarcane straw	44.80 ± 0.1	5.94 ± 0.03	0.10 ± 0.02	48.89 ± 0.1	0.27 ± 0.01	17.01	15.71
Rice husk	40.82 ± 0.3	5.25 ± 0.03	0.38 ± 0.01	53.38 ± 0.2	0.17 ± 0.03	16.63	14.89
Shea butter wood	50.03 ± 0.1	6.30 ± 0.03	0.11 ± 0.02	43.54 ± 0.1	0.02 ± 0.01	23.10	21.73
Palm kernel shell	48.28 ± 0.1	5.39 ± 0.03	0.12 ± 0.02	46.18 ± 0.1	0.03 ± 0.01	21.65	20.47
Bamboo wood	45.02 ± 0.3	5.91 ± 0.03	0.30 ± 0.01	48.58 ± 0.2	0.19 ± 0.001	18.86	17.57

C: Carbon, **H**: Hydrogen, **N**: Nitrogen, **O**: Oxygen, **S**: Sulphur, **HHV**: Higher heating value (MJ/kg), **LHV**: Lower heating value (MJ/kg).

Table 12: Structural composition analysis of selected biomass samples [11].

Sample	**Ce (%)**	**He (%)**	**Li (%)**	**Ee (%)**	**Co**
Siam weed	25.32 ± 1.06	26.60 ± 0.20	29.60 ± 0.62	0.49 ± 0.02	0.00100
Gmelina arborea	45.30 ± 1.08	28.15 ± 0.20	25.70 ± 0.59	0.25 ± 0.01	0.00113
Sugarcane straw	40.99 ± 0.93	27.49 ± 0.10	20.75 ± 0.40	0.73 ± 0.02	0.00100
Rice husk	36.56 ± 0.82	20.12 ± 0.20	19.44 ± 0.20	0.20 ± 0.02	0.00113
Shea butter wood	44.80 ± 0.11	30.94 ± 0.20	23.82 ± 0.30	0.44 ± 0.02	0.00100
Palm kernel shell	28.92 ± 0.14	25.01 ± 0.10	45.41 ± 0.40	0.65 ± 0.02	0.00100
Bamboo wood	40.96 ± 0.92	25.83 ± 0.20	21.96 ± 0.20	0.25 ± 0.02	0.00303

Ce: Cellulose, **He**: Hemicellulose, **Li**: Lignin, **Ee**: Ether extract, **Co**: Corrosiveness index.

Table 13: Mean composition of pine wood. Data from Phyllis database [12]

	Pine
Volatiles [% daf]	80.48
Fixed carbon [% daf]	19.52
Ash [% dry]	0.6
C [% daf]	52.11
H [% daf]	6.14
O [% daf]	41.44
N [% daf]	0.3
S [% daf]	0.01
Cellulose [% dry]	45.00
Hemicellulose [% dry]	27.50
Lignin [% dry]	25.00
LHV [MJ $kg^{-}1$ daf]	20.87

B Technical data reference engines

B.1 Biomass-fuelled engine

Engine information	1D81
Type	Air-cooled 4 stroke diesel engine
Compression ratio	21.5
Speed	1500-3000 rpm
Injection	Direct injection
Number of cylinder	1
Bore &Stroke [mm]	100 & 85
Displacement [cm^3]	667

Table 14: Technical data Hatz 1D81 [13]

Phase	Compression	Ignition	Combustion	Extinction
Temperature [K]	$373 \rightarrow 453$	$453 \rightarrow 673$	$673 \rightarrow 973$	$973 \rightarrow 373$
Pressure [bar]	$2 \rightarrow 4$	$4 \rightarrow 30$	$30 \rightarrow 60$	$120 \rightarrow 1$
Duration [ms]	3	4	2	17.77
Heating rate [K/s]	26.66e3	55e3	150e3	-33.75e3

Table 15: Gas heating steps during a Hatz 1D81 engine cycle (1500 rpm) running with biomass [14]

B.2 Diesel-fuelled engine

Engine type	Single cylinder
Injection	Direct injection
Compression ratio	17.5
Speed	900-2100 rpm
Fuel	Diesel
Bore & Stroke	80 mm & 110 mm
Displacement [cm^3]	552
Injected duration [CAD]	21.5 before TDC

Table 16: Technical data engine from [9]

Peak temperature for 1000 rpm engine speed is extrapolated at 2650 K. The peak temperatures for 1200 and 1500 rpm are 2920 K and 3278 K respectively. In-cylinder peak pressure is set to the same value for each engine speed and is equal to 154 bar.

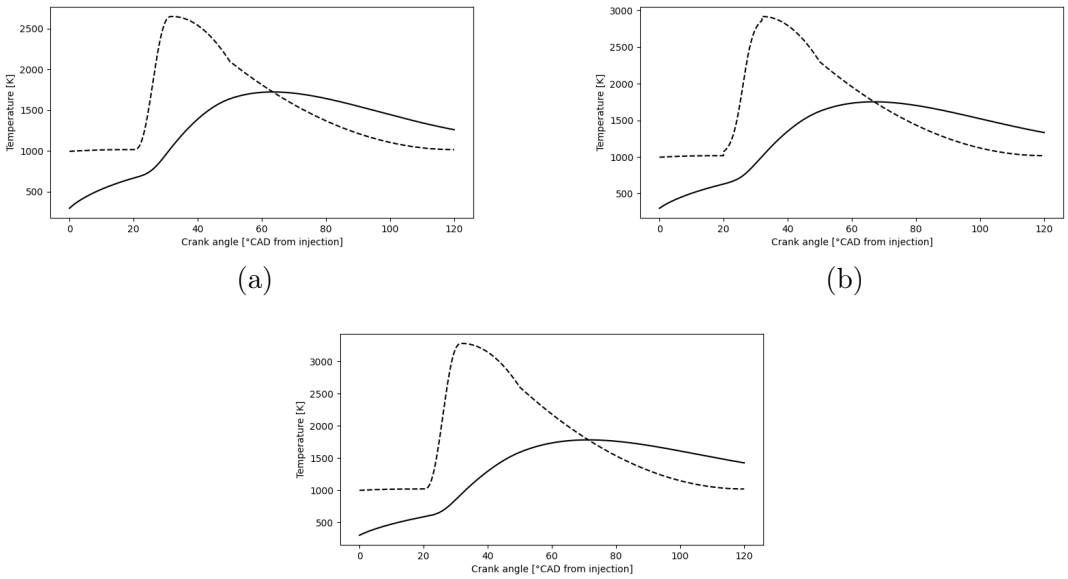

Figure 16: Temperature profiles for various engine speed for a 30μm particle radius. In-cylinder gas temperature (dashed) and Particle surface temperature (solid) vs. CAD (after injection). 1000 rpm (a), 1200 rpm (b) and 1500 rpm (c).

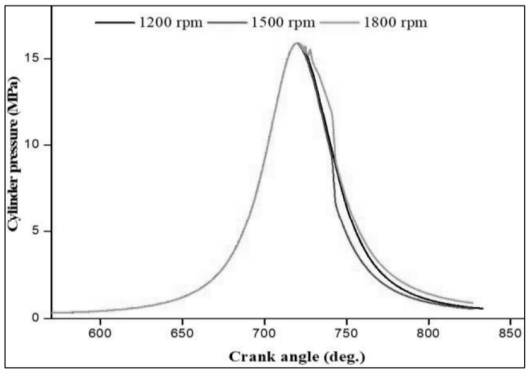

Figure 17: Pressure vs. Crank angle from [9].

C Fixed surface temperature scenario

This scenario was computed at the beginning of this work and is presented here solely for completeness.

This scenario do not present the real internal combustion engine conditions but it gives a relevant first sight about the conversion rate influenced by the temperature and particle size at atmospheric pressure.

In summary, the temperature profile consists of two main stages:

1. Initially, the bulk gas temperature increases from 373 K to 973 K (characteristic temperature from [14]), following three distinct heating rates illustrated in Table 15. During this phase, the particle heats up via a convective heat flux, which depends on both the gas temperature and a heat transfer coefficient related to the particle radius defined with Equation 5.6.

2. Subsequently, the bulk gas temperature remains constant at 973 K. The particle continues to heat up by convection until it reaches thermal equilibrium with the gas. Once this equilibrium is attained, its temperature remains stable for the rest of the simulation.

In this configuration, the pyrolysis process does not show a well-defined termination. As the ambient temperature continuously rises and remains elevated throughout the entire simulation, the particle mass keeps decreasing even after the 80 ms simulation window, corresponding to a full engine cycle at 1500 rpm engine speed. In Figure 19a, the initial drop in mass is associated with the drying phase, given that the pinewood particle enters the combustion chamber with an initial moisture content of 8%. The subsequent sharp decrease is attributed to the release of volatiles from the thermal degradation of lignocellulosic compounds. This is followed by a longer and relatively constant decline, reflecting the slow emission of remaining volatile species. Notably, no secondary peak corresponding to light gases and tar release is observed in this case. This absence can be attributed to the fact that the particle's temperature does not reach the required level to allow the release of the trapped species. The end of the pyrolysis is assumed to occur at t=80 ms, from which the relative residual mass fraction is determined. Larger particles exhibit higher residual mass fractions, as it requires more time for the particles to reach sufficiently high temperatures, resulting in slower reaction rates.

The surface temperature of the particle rapidly reaches the limiting value for diameters smaller than 100 μm, providing a preliminary indication of the critical particle size. At this threshold diameter, the particle requires significantly more time to heat up, which prolongs the pyrolysis process and ultimately leads to a higher residual mass fraction entering the char oxidation phase. Although, during oxidation, the particle is nearly at (or has already reached) the maximum temperature of 973 K (in this particular scenario), the thick particle (d = 100μm) consistently exhibits the slowest reaction rate. This behaviour indicates that the Biot number exceeds 0.1, confirming that the particle cannot be assumed to be thermally thin.

As expected, under such low-temperature conditions, complete combustion would require more than 120 ms for the smallest particle and nearly 240 ms for the largest one. The objective here, however, is to highlight that, under identical conditions, particle size has a significant influence on the time required for reaction completion.

	Radius [μm]	t_{end} [ms]	$T_{\text{p,start}}$ [K]	$T_{\text{p,end}}$ [K]	Initial mass [kg]	m_{res}/m_0 [%]
Pyrolysis	10	80	298	973	0.0025e-10	12.33
	12	80	298	973	0.0044e-10	12.33
	15	80	298	973	0.0085e-10	12.42
	20	80	298	973	0.0201e-10	12.68
	50	80	298	969.2	0.3147e-10	19.38
Char oxidation*	10	43.10	973	973	0.030e-12	0.0
	12	52.10	973	973	0.054e-12	0.0
	15	65.90	973	973	0.104e-12	0.0
	20	89.50	973	973	0.247e-12	0.0
	50	262.4	969.2	973	6.100e-12	0.0

Table 17: Numerical results under fixed surface temperature scenario.
*The radius is shown here for clarification; in reality, it differs between the pyrolysis and oxidation phases.

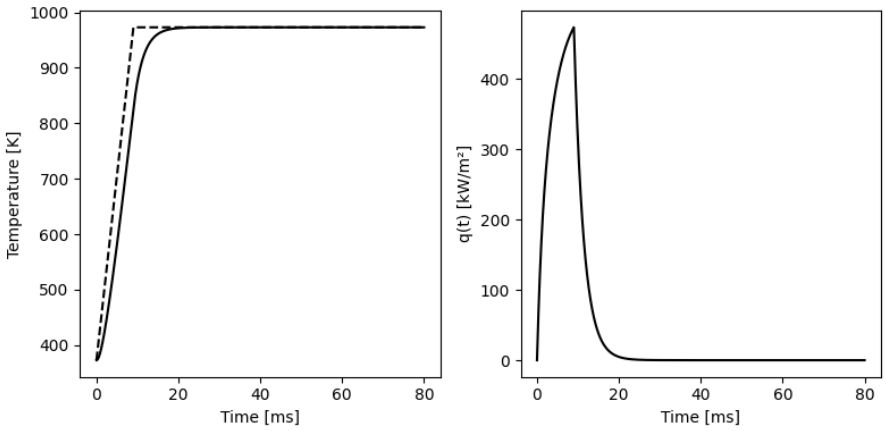

Figure 18: Fixed surface temperature. (Left) Gas temperature (dashed) and Particle surface temperature (solid) vs. time for a particle radius of 20 μm, $h_{conv} = 3150$ $Wm^{-2}K^{-1}$. (Right) Convective heat flux applied to the particle vs. time.

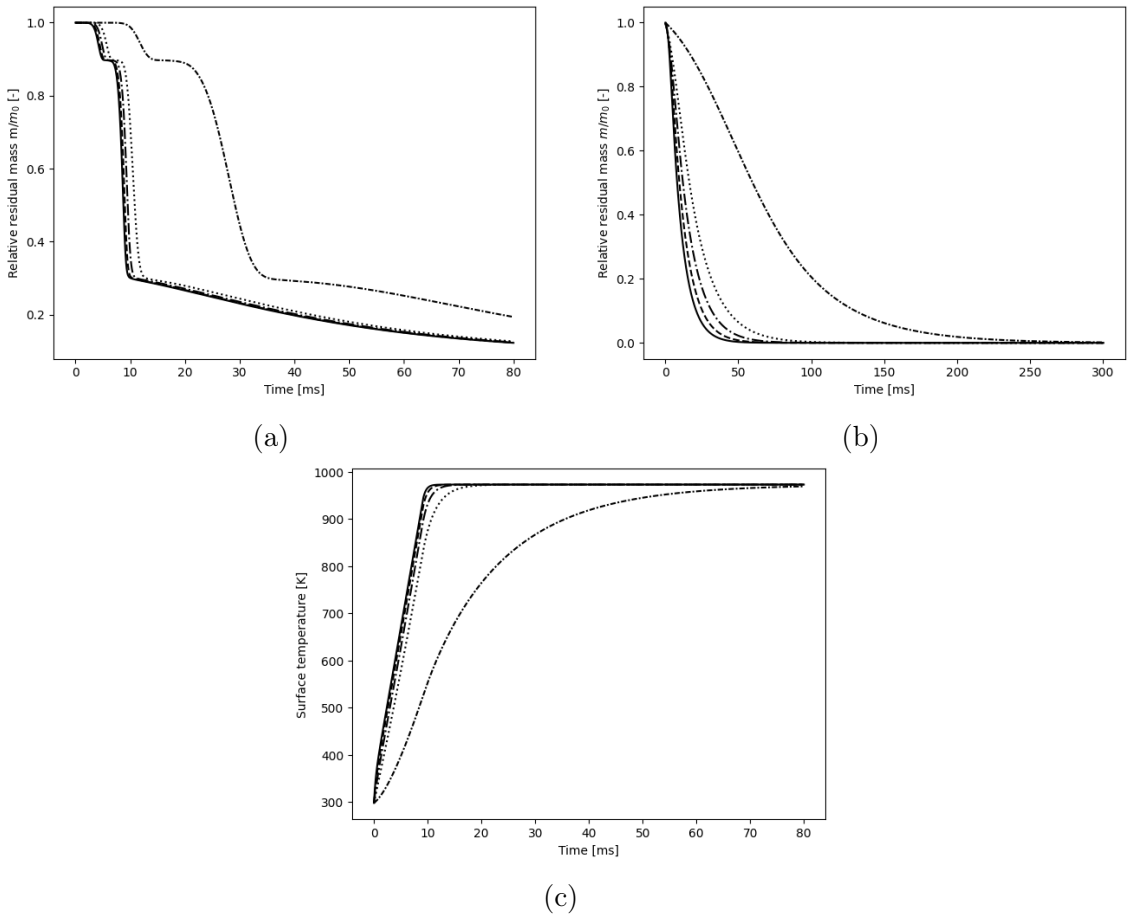

Figure 19: Graphs for the fixed temperature scenario for three different particle radii: 10μm (solid),12μm (dashed),15μm (dashdot), 20μm (dotted) and 50μm (shorter dashdot). (a) Pyrolysis computed with SPY. (b) Oxidation of the remaining fixed carbon content. (C) Temperature profile

References

[1] C. Jensen, J. Guerrero, S. Karatzos, G. Olofsson, and S. Iversen, "Fundamentals of hydrofaction™: Renewable crude oil from woody biomass," *Biomass Conversion and Biorefinery*, 7, 2017.

[2] B. Piriou, G. Vaitilingom, B. Veyssière, B. Cuq, and X. Rouau, "Potential direct use of solid biomass in internal combustion engines," *Progress in Energy and Combustion Science*, 39/169-188, 2013.

[3] H. Lu., *Experimental and modeling investigations of biomass particle combustion.* PhD thesis, PhD thesis, Brigham Young University, 2006.

[4] J. Blondeau, *Investigation of pulverised biomass combustion: detailed modelling of particle pyrolysis and experimental analysis of ash deposition.* PhD thesis, Université catholique de Louvain, May 2013.

[5] P. L. W. JR., F. R. JR., and L. G. AUSTIN, "Gas reaction of carbon," *Advances in Catalysis*, 11/133-221, 1959.

[6] H. E. KLIMESH and R. H. ESSENHIGH, "Non-dissociative and dissociative adsorption of oxygen on carbon: A theoretical comparison with prediction of reaction order," *Twenty-Seventh Symposium (International) on Combustion/The Combustion Institute*, 2941–2948, 1998.

[7] M. Cieplik, L. Fryda, W. van de Kamp, and J. Kiel, "Ash formation, slagging and fouling in biomass co-firing in pulverised-fuel boilers," *Solid Biofuels for Energy*, 9/197-217, 2010.

[8] D. D. Toporov, "Mathematical modelling and model validations," *Combustion of Pulverised Coal in a Mixture of Oxygen and Recycled Flue Gas*, 4/51-97, 2014.

[9] U. Rajak and T. N. Verma, "Influences of engine speed variations on single cylinder direct injection diesel engine," *ADVANCES IN ENGINEERING TECHNOLOGY*, 4/61-71, 2019.

[10] V. Doshi, H. Vuthaluru, R. Korbee, and J. Kiel, "Development of a modeling approach to predict ash formation during co-firing of coal and biomass," *Fuel processing technology*, 90/1148-1156, 2009.

[11] A. O. et al., "Characterization of lignocellulose biomass based on proximate, ultimate, structural composition, and therm analysis," *Material Todays: Proceedings*, 65/2156-2162, 2022.

[12] E. research Centre of the Netherlands (ECN), "Phyllis2 - ecn phyllis classification." Website https://phyllis.nl/Browse/Standard/ECN-Phyllis.

[13] M. Hatz, "Diesel engine," *Manual*, 2023.

[14] L. Stover, C. Caillol, B. Piriou, C. Mayer-Laigle, X. Rouau, and G. Vaïtilingom, "A phenomenological description of biomass powder combustion in internal combustion engines," *Energy*, 2023.

[15] C. Deheri, S. K. Acharya, D. N. Thatoi, and A. P. Mohanty, "A review on performance of biogas and hydrogen on diesel engine in dual fuel mode," *Fuel*, 260, 2020.

[16] C. Zhang, N. Liu, T. Zhang, S. Su, R. Li, J. Feng, and Y. Wu, "Influence of biomass type and pyrolysis temperature on biochar characteristics for enhanced soil amendment," *Journal of Analytical and Applied Pyrolysis*, 192, 2025.

[17] N. T. Setioputro, Muchammad, E. Yohana, Syaiful, H. D. Ariyanto, and M. Kosim, "Effect of soaked biomass on gasification temperature performance in an open-downdraft gasifier," *Bioresource Technology*, 415, 2025.

[18] F. Wang, D. Ouyang, Z. Zhou, S. J. Page, D. Liu, and X. Zhao, "Lignocellulosic biomass as sustainable feedstock and materials for power generation and energy storage," *Journal of Energy Chemistry*, 57/247-280, 2021.

[19] X. C. et al., "Moisture content effects on self-heating in stored biomass: An experimental study," *Energy*, 285, 2023.

[20] H. Mohanna, *Combustion of pulverized biomass impact of fuel preparation and flow conditions*. PhD thesis, PhD thesis, INSA Rouen Normandie, 2020.

[21] J. Woodworks, "Drying times for fresh cut timber by species." December 2023.

[22] E. Alakangas, "Biomass and agricultural residues for energy generation," *Fuel Flexible Energy Generation*, 3/59-96, 2016.

[23] fire & safety center, "Auto ignition temperature." Website https://www.fireandsafetycentre.co.uk/blogs/safety-storage/auto-ignition-temperature.

[24] V. Soloiu, J. Lewis, Y. Yoshihara, and K. Nishiwaki, "Combustion characteristics of a charcoal slurry in a direct injection diesel engine and the impact on the injection system performance," *Fuel and Energy Abstracts*, 36/4353-4371, 2011.

[25] L. Li, J. S. Rowbotham, H. C. Greenwell, and P. W. Dyer, "An introduction to pyrolysis and catalytic pyrolysis: Versatile techniques for biomass conversion," *New and Future Developments in Catalysis*, 8/173-208, 2013.

[26] G. K. Nayak, M. N. Popov, and D. Holec, "Pressure- and temperature-dependent diffusion from first-principles: A case study of v and ti in a tin matrix," *Surface & Coatings Technology*, 422, 2021.

[27] J. Tomeczek and S. Gil, "Volatiles release and porosity evolution during high pressure coal pyrolysis," *Fuel*, 82/285-292, 2003.

[28] M. Aliramezani, C. R. Koch, and M. Shahbakhti, "Modeling, diagnostics, optimization, and control of internal combustion engines via modern machine learning techniques: A review and future directions," *Progress in Energy and Combustion Science*, 88, 2022.

[29] C. Belviso, "State-of-the-art applications of fly ash from coal and biomass: A focus on zeolite synthesis processes and issues," *Progress in Energy and Combustion Science*, 65/109-135, 2018.

[30] Salomóna, Marianne, Savola, Tuula, Martin, Andrew, Fogelholm, Carl-Johan, Fransson, and Torsten, "Small-scale biomass chp plants in sweden and finland," *Renewable & Sustainable Energy Reviews - RENEW SUSTAIN ENERGY REV*, 15/4451-4465, 2011.

[31] W. Louis, P. Doug, and S. Peter, "Efficient use of coal water fuels," *CCSD - Australian CSIRO*, 2008, Report number: 74.

[32] R. Patton, P. Steele, and F. Yu, "Coal vs. charcoal-fueled diesel engines: A review," *Energy Sources*, 315-322, 2010.

[33] G. S. et al., "Principles for the design of a biomass-fueled internal combustion engine," *Energies*, 17/1700, 2024.

[34] A. Rentizelas, "Biomass storage," *Biomass Supply Chains for Bioenergy and Biorefining*, 6/127-146, 2016.

[35] X. Pan, W. Lian, J. Yang, J. Wang, Z. Zhang, X. Hao, A. Abudula, and G. Guan, "Downer reactor simulation and its application on coal pyrolysis: A review," *Carbon Resources Conversion*, 5/35-51, 2022.

[36] A. K. Vuppaladadiyam, S. S. V. Vuppaladadiyam, A. Abhishek, R. S. Sahoo Abhisek, P. K. Kishore, M. S., H. Qing, A. Edward, F. Paul, B. Sankar, and L. Shao-Yuan, "Biomass pyrolysis: A review on recent advancements and green hydrogen production," *Bioresource Technology*, 2022.

[37] S. Boraste, "Drying." Website https://fr.slideshare.net/slideshow/drying-238148512/238148512 (p.5).

[38] A. Demirbas, "Relationships between lignin contents and fixed carbon contents of biomass samples," *Energy Conversion and Management*, 44/1481–1486, 2002.

[39] Q. W. et al., "Effect of pressure on the pyrolysis and gasification mechanism of corn stovers from kinetics," *Journal of Analytical and Applied Pyrolysis*, 176, 2023.

[40] Z. Guo, W. Zhou, Y. Liu, X. Li, B. Bai, F. Li, C. Luo, and G. Yang, "Effect of pyrolysis temperature on migration characteristics of heavy metals during biomass pyrolysis," *Journal of the Energy Institute*, 117, 2024.

[41] E. Ranzi, A. Cuoci, T. Faravelli, A. Frassoldati, G. Migliavacca, S. Pierucci, and S. Sommariva, *Chemical kinetics of biomass pyrolysis.* Energy and Fuel, 22/4292-4300, 2008.

[42] E. ToolBox, "Air properties - thermal conductivity vs. temperature and pressure charts and calculator." $https : //www.engineeringtoolbox.com/air - properties - viscosity - conductivity - heat - capacity - d_1509.html$.

[43] I. Ismail, E. Abdelrazek, M. Ismail, and A. Emara, "An investigation study of the thermomechanical loading on the piston of a diesel engine with design improvements," *SAE Technical Paper*, 2020-01-5098.

[44] C. Guillaume, "Sustainability in the cement industry: Substitution of coal for biomass," Master's thesis, Ecole Polythechnique de Louvain (EPL), 2014.

[45] C. R. MONSON, G. J. GERMANE, A. U. BLACKDAM, and L. D. SMOOT, "Char oxidation at elevated pressures," *Combustion and Flame*, Volume 100, Issue 4, Pages 669-683, 1995.

[46] S. . E. Cornell Composting, "Calculating the oxygen diffusion coefficient in air." Website https://compost.css.cornell.edu/oxygen/oxygen.diff.air.html.

[47] Q. Ye, C. Li, T. Yang, Y. Wang, Z. Li, and Y. Yin, "Relationship between desorption amount and temperature variation in the process of coal gas desorption," *Fuel*, 332, 2023.

[48] W. C. H. J. HONG and T. H. FLETCHER, "Modeling high-pressure char oxidation using langmuir kinetics with an effectiveness factor," *Proceedings of the Combustion Institute*, 28/2215-2223, 2000.

[49] J.-M. Commandre, "Formation des oxydes d'azote lors de la combustion de cokes de pétrole dans des conditions de précalcinateur de cimenterie," Master's thesis, Institut National Polytechnique de Toulouse, 2002.

[50] E. Thiele, "Relation between catalytic activity and size of particle," *Ind. Eng. Chem*, 31/916-920, 1939.

[51] Z. Tan and A. Lagerkvist, "Phosphorus recovery from the biomass ash: A review," *Renewable and Sustainable Energy Reviews*, 15/3588-3602, 2011.

[52] V. Soloiu, J. Lewis, Y. Yoshihara, and K. Nishiwaki, "Combustion characteristics of a charcoal slurry in a direct injection diesel engine and the impact on the injection system performance," *Energy*, 36/4353-4371, 2011.

[53] R. Zhang, Y. Chen, K. Lei, and D. Liu, "The effects of specific surface area and ash on char gasification mechanisms in the mixture of h2o, co2, h2 and co," *Fuel*, 209/109-116, 2017.

[54] C. E. Brewer, V. J. Chuang, C. A. Masiello, H. Gonnermann, X. Gao, B. Dugan, L. E. Driver, P. Panzacchi, K. Zygourakis, and C. A. Davies, "New approaches to measuring biochar density and porosity," *Biomass and Bioenergy*, 66/176-185, 2014.

[55] W. B. FU, B. L. ZHANG, and S. M. ZHENG, "A relationship between the kinetic parameters of char combustion and the coal's properties," *Combustion and flame*, 109/587-598, 1997.

[56] T. KASHIWAGI and H. NAMBU, "Global kinetic constants for thermal oxidative degradation of a cellulosic paper," *Combustion and flame*, 8/345-368, 1992.

[57] A. G. M. B. Mustayen, X. Wang, M. Rasul, J. Hamilton, and M. Negnevitsky, "Thermodynamic analysis of diesel engine ignition delay under low load conditions," *Energy Reports*, 8/495-501, 2022.

[58] L. Bates, D. Bradleya, G. Paczko, and N. Peters, "Engine hot spots: Modes of auto-ignition and reaction propagation," *Combustion and Flame*, 166/80-85, 2016.

UNIVERSITÉ CATHOLIQUE DE LOUVAIN
École polytechnique de Louvain
Rue Archimède, 1 bte L6.11.01, 1348 Louvain-la-Neuve, Belgique | **www.uclouvain.be/epl**